Environmental Science Nano

Evaluation of Labeling Methods Used for Investigating the Environmental Behavior and Toxicity of Metal Oxide Nanoparticles

Journal:	*Environmental Science: Nano*
Manuscript ID	EN-CRV-10-2018-001187.R1
Article Type:	Critical Review
Date Submitted by the Author:	30-Jan-2019
Complete List of Authors:	Deline, Alyssa; Johns Hopkins University, Department of Chemistry Nason, Jeffrey; Oregon State University, Chemical, Biological and Environmental Engineering

Environmental Significance Statement for "Evaluation of Labeling Methods Used for Investigating the Environmental Behavior and Toxicity of Metal Oxide Nanoparticles"

Alyssa R. Deline and Jeffrey A. Nason

Understanding the potential toxicity and environmental impact of metal oxide nanoparticles (MONPs) requires that researchers study MONPs at environmentally-relevant concentrations in complex, real-world systems. However, high background concentrations of the metals of interest are present in every environmental compartment as well as many organisms. To address this challenge, researchers have developed a suite of labeling strategies that allow for the enhanced detection and quantification of engineered MONPs. This includes fluorescent dye labels, stable and radioactive isotopes, dopants, and core/shell labels. This paper provides guidance on choosing the most advantageous labeling technique for a desired research application, as well as recommendations for rigorous characterization of labeled MONPs and the reporting of key label parameters.

Evaluation of Labeling Methods Used for Investigating the Environmental Behavior and Toxicity of Metal Oxide Nanoparticles

Alyssa R. Deline and Jeffrey A. Nason

School of Chemical, Biological and Environmental Engineering, Oregon State University

116 Johnson Hall, Corvallis, Oregon 97331, United States

Abstract

The analysis of the environmental behavior and toxicity of metal oxide nanoparticles (MONPs) is complicated by high metal concentrations in natural matrices. To better detect and quantify MONPs in complex samples, a variety of traceable labels can be incorporated. There are four primary categories of MONP labels: fluorescent dyes, radioisotopes, stable isotopes, and dopant/core-shell labels. This review describes each MONP labeling technique, along with its advantages and drawbacks, and provides strategies for choosing the most appropriate labeling method for a given study design.

Introduction

Metal oxide nanoparticles (MONPs) are produced and applied at the highest rate of any class of nanomaterial, inspiring a growing body of research on the potential impact of MONPs to the environment and human health[1]. The broad category of "MONP" describes any nanoparticle with an inorganic core composed of a metallic element bonded to oxide (O^{2-}) anions. MONPs are used in a variety of applications, including paints and coatings, sunscreens, chemical mechanical planarization, personal care products, antimicrobial treatments, and catalysis[2,3].

A considerable amount of work has focused on studying the toxicity of MONPs, especially the commonly produced transition metal oxides silicon dioxide (SiO_2 NPs), titanium dioxide (TiO_2 NPs), zinc oxide (ZnO NPs) and copper oxide (CuO NPs). The general trend of reported toxicities to mammalian cell lines and microbes is CuO NPs > ZnO NPs > TiO_2 NPs > SiO_2 NPs[4–11]. Nanomaterials composed of iron oxides (FeO_x NPs), cerium dioxide (CeO_2), and aluminum oxide (Al_2O_3 NPs) are typically regarded as nontoxic[11–14], but in some cases have been shown to induce inflammatory responses[15–18]. There are several relevant mechanisms of toxicity. In photocatalytically active MONPs like TiO_2, the production of reactive oxygen species (ROS) is the cause of the toxic response, while in soluble MONPs like ZnO and CuO, the response is primarily caused by the release of toxic metal ions[19,20]. MONPs that do not generate ROS or release ions can still cause toxicity through interactions with cell membrane surfaces or uptake into cells[21]. While MONP toxicity is well understood in single organism studies, more work needs to be done to understand MONP toxicity in the complex multi-organism scenarios that would more accurately represent natural systems.

MONPs have a wide range of physicochemical, structural, and electronic properties that contribute to their exposure pathway and toxicity toward organisms. Predictive models for MONP toxicity are difficult to develop, as the relevant particle properties are heavily dependent on the surrounding environment[22]. It is therefore vital that MONP behavior is studied in matrices that reflect real-world complexity; yet, this is uniquely challenging due to natural background concentrations of elements found in MONPs. Metal oxides of interest in nanotoxicology also exist in large quantities as natural minerals in the Earth's crust[23]. Additionally, some of the corresponding metallic elements (e.g., Zn, Cu) are present in organisms as elements essential for nutrition[24]. Table 1 summarizes the disparities between the background concentrations of metals

in the environment and the expected concentrations and production rates of the most common MONPs. It is clear that MONP concentrations in most samples can be expected to be several orders of magnitude lower than concentrations of naturally occurring metals and metal oxides, complicating detection and quantification.

Table 1. Estimated MONP and background metal concentrations.

MONP	Background Metal Concentration	MONP Production Rate	Estimated MONP Concentration
SiO_2	270 g/kg in Earth's crust[25] 2.81 mg/L in oceans[26] 5.42 mg/L in rivers[27] 10 µg/kg in human body[28]	5,500 t/yr [2]	
TiO_2	5.0 g/kg in Earth's crust[25] 0.48 µg/L in oceans[26] 0.489-10 µg/L in rivers[27,29]	3,000 t/yr [2]	3 ng/L - 1.6 µg/L in river water[30]; 1.4 - 10.8 µg/L in WWTP effluent[30,31]
ZnO	79 mg/kg in Earth's crust[25] 0.41 µg/L in oceans[26] 0.60-30 µg/L in rivers[27,29] 2.0 µg/kg in human body[28]	550 t/yr [2]	1 - 55 ng/L in river water[31]; 0.22 – 1.42 µg/L in WWTP effluent[31]
Al_2O_3	83 g/kg in Earth's crust[25] 0.54 µg/L in oceans[26] 50 µg/L in rivers[27] 0.1 µg/kg in human body [28]	55 t/yr [2]	
FeO_x	69 g/kg in Earth's crust[25] 0.06 µg/L in oceans[26] 40-66 µg/L in rivers[27,29] 10 µg/kg in human body[28]	55 t/yr [2]	
CeO_2	32 mg/kg in Earth's crust[25] 0.0028 µg/L in oceans[26] 0.08-0.262 µg/L in rivers[27,29]	55 t/yr [2]	
CuO	79 mg/kg in Earth's crust[25] 0.25 µg/L in oceans[26] 1.48-10 µg/L in rivers[27,29] 0.1 µg/kg in human body[28]	> 150 t/yr [3]	

Background metal concentrations for rivers and oceans represent the estimated world average concentration in the dissolved fraction.

Several analytical techniques have been developed to address the challenge of studying nanomaterials in complex matrices, but limitations remain for each strategy[32,33]. Field-flow fractionation (FFF) techniques have been used to separate particles in suspension by size or relative density, providing sensitive sample fractionation for the identification of nano-sized materials in real-world samples[34,35]. When coupled with a detector like inductively coupled plasma-mass spectrometry (ICP-MS), FFF allows researchers to determine the size and mass

distribution of MONPs in samples like commercial sunscreens and natural waters[36,37]. Single particle ICP-MS (sp-ICP-MS) methods have been used to provide the MONP number concentration and size distribution in complex samples[38,39]. Both of these techniques are limited by the inability to distinguish engineered MONPs from natural colloids in the nano-size range, and by the confounding effects of particle dissolution[40]. Another drawback for sp-ICP-MS is that the minimum particle size for detection is in the 20-80 nm range for most MONPs, and above 200 nm for SiO_2 NPs[41].

One technique that addresses the challenge of discerning between engineered and natural colloids is the strategy of comparing bulk isotopic ratios within the MONP to those found in the natural environment, or comparing the bulk ratio of the MONP metal to a concomitant element[32,42,43]. However, this method of comparing elemental and isotopic ratios cannot be applied when there is no appropriate ratio to utilize, and the high background concentration of metals in the environment make small fluctuations in bulk ratios difficult to identify with accuracy. Recently, multi-element single particle inductively coupled plasma time-of-flight mass spectrometry (sp-ICP-TOF-MS) has been used to examine elemental ratios within individual nanoparticles[43,44]. Engineered CeO_2 NPs were successfully distinguished from natural Ce containing particles using this method[43], but there was no clear fingerprint that could be used for engineered TiO_2 NPs[44]. One drawback of this method is that there is currently no way to identify nanosized particles that are present in larger heteroaggregates[44].

Visualization techniques have also been used to identify MONPs in complex matrices. Both scanning electron microscopy (SEM) and transmission electron microscopy (TEM) have been applied to visualize MONPs in a variety of samples including fibroblast cells, commercial sunscreens, and food products[45–47]. One drawback of using SEM/TEM techniques is that there is

often a qualitative determination that an observed particle is engineered versus naturally occurring based on particle morphology, even when energy dispersive x-ray (EDS/EDX) analysis is used to verify the elemental composition of particles within a sample. In some cases, the presence of a concomitant element may be used to assist in this determination, just as elemental ratios are used in ICP-MS techniques. Another drawback is that statistically-significant particle counts are time consuming and expensive to acquire. An additional visualization technique is atomic force microscopy (AFM), which can be used to characterize the morphology and distribution of MONPs in a sample[46,48]. However, particle size distributions cannot be truly quantitatively determined using AFM alone. Synchotron-based techniques have been used to study TiO_2 in sewage sludge, soil, and sludge-amended soil[49]. X-ray absorption near edge structure (XANES) spectroscopy, micro and nano X-ray fluorescence (μXRF and nanoXRF) and Ti K-edge microXANES spectroscopy were used in combination in an attempt to determine whether the Ti content, particle size distribution, or Ti speciation could be used to distinguish anthropogenic TiO_2 NPs from naturally occurring materials. None of these properties proved effective, and the authors recommended future work examining the morphology of the TiO_2 NPs and their presence within larger aggregates as potential criteria for identification[49].

For SEM, TEM, AFM, and synchrotron-based analyses, it is vital that samples are prepared with care to limit the incorporation of experimental artefacts. It is also important to note that as engineered MONPs are weathered in a complex matrix, the morphological differences between the natural and engineered particles may lessen over time, which could result in the false assignment of these particles as naturally occurring metal oxides[49]. Overall, the application of each of these quantification and visualization techniques for examining MONPs in natural

systems requires considerable improvement in the ability to detect minute MONP concentrations against a complex background containing naturally occurring metals and metal oxides.

To address these limitations in current analytical methods, a traceable label can be incorporated into MONPs to distinguish them from the sample background. This allows for the sensitive detection of engineered nanomaterials in the size range of interest even when natural colloids of the same metallic composition are present within the sample. To be effective, the presence of the label cannot change the relevant properties and behavior of the MONP, and it must enable the quantification and/or visualization of the engineered MONPs at environmentally relevant concentrations. In this critical review we describe existing MONP labeling techniques in detail, analyze the benefits and disadvantages of each, identify gaps in the current body of literature, and provide guidelines for choosing the most appropriate labeling method.

Many of the labeling, characterization, and quantification techniques explored in this paper can be applied to a variety of nanomaterial categories and are not restricted solely to MONPs. However, MONPs are the focus of this review because they epitomize the intersection of high rates of release into the environment and a high susceptibility to background interference, which are key concerns in the study of the environmental behavior of nanomaterials. As such, this review is also limited to MONP labeling applications relevant to investigating toxicological impact and environmental transport. While it is important to note that additional MONP labeling procedures have also been developed for applications in biomedical imaging and nanomedicine, they are not included in this review. This is because these MONPs are often functionalized for biocompatibility and targeted transport to a specific organ, making them unsuitable for environmental studies where the properties should match the more widely applied commercially available MONPs that do not undergo such functionalization[50]. Ultimately, the goal of this

review is to provide an in-depth discussion of the details of synthesis, characterization, and utility that is necessary for researchers to effectively choose and apply a MONP labeling strategy.

To achieve this goal, this review has been formatted as summarized in Schematic 1. We begin with a summary of each of four categories of MONP labels that outline synthetic techniques, quantification, experimental design considerations, notable examples and advantages and disadvantages. The next major section is focused on the potential impacts that labels can have on MONP properties and the techniques available for evaluating those effects. Finally, we provide guidance on choosing the optimal labeling strategy for a specific experiment and model the decision-making process using case-studies.

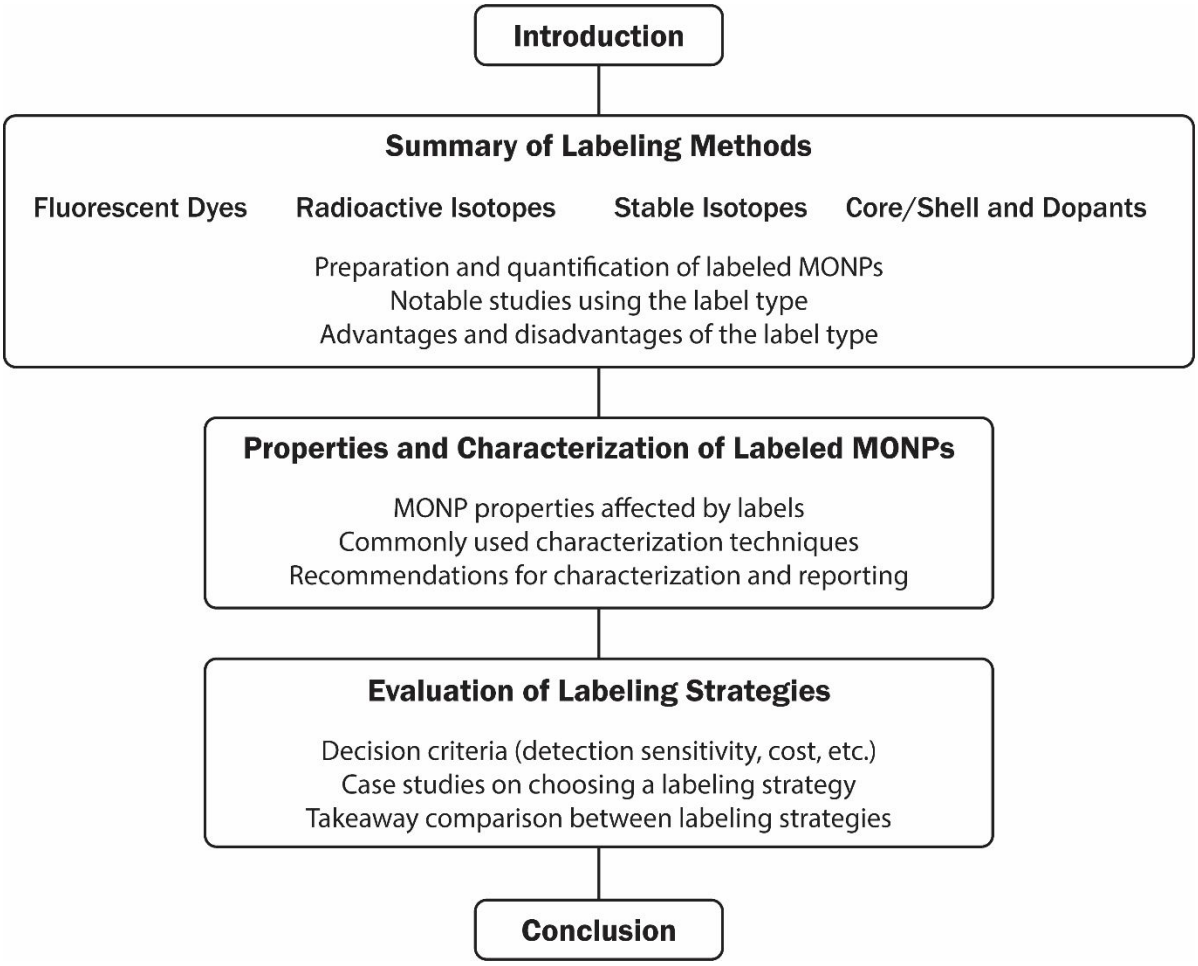

Schematic 1. Format of this review article.

Summary of Labeling Methods

Fluorescent Dye Labels

The most common MONP labeling technique is the incorporation of a fluorescent dye. There are several synthetic routes that are used to produce fluorescent dye labeled MONPs, as summarized in Figure 1. One method is to covalently attach a fluorescent dye to the surface of a previously synthesized or purchased MONP using an aminosilane coupling agent. SiO_2, TiO_2, CeO_2 NPs, and ZnO NPs labeled with fluorescein isothiocyanate (FITC) have each been prepared using this method[11,51]. MONPs can also be doped with fluorescent dyes throughout the

particle structure using a modification of existing sol-gel[51,52] or microemulsion[53,54] synthetic processes. Here, the dye is mixed into the synthetic solution that containing the metal-alkyl precursor. Optionally, the dye-doped MONP can then be coated with an undoped metal oxide shell[50,51,55]. Another method of producing core@shell fluorescent MONPs is the amino acid-catalyzed seed regrowth technique (ACSRT), in which amino acids drive the production of densely doped seeds, then additional metal-alkyl precursor is added to form a shell[56–58]. Each of these dye-doping and core@shell methods have been used primarily to label SiO_2 NPs, but could be extended to other MONPs. While the surface attachment approach has the benefit of applicability to commercially available MONPs, it introduces both the silane coupling agent and the fluorescent dye to the surface of the MONP of interest, which could potentially impact particle surface properties or lead to the premature release of dye. Coating fluorescently-doped SiO_2 seeds with an unlabeled SiO_2 shell has been shown to limit the release of dye, as has the employment of an amino acid catalyst in the hydrolysis reaction [57–59]. A combination of these two approaches resulted in fluorescent dye leakages of below 5% after a 72 hour exposure to high ionic strength media[57].

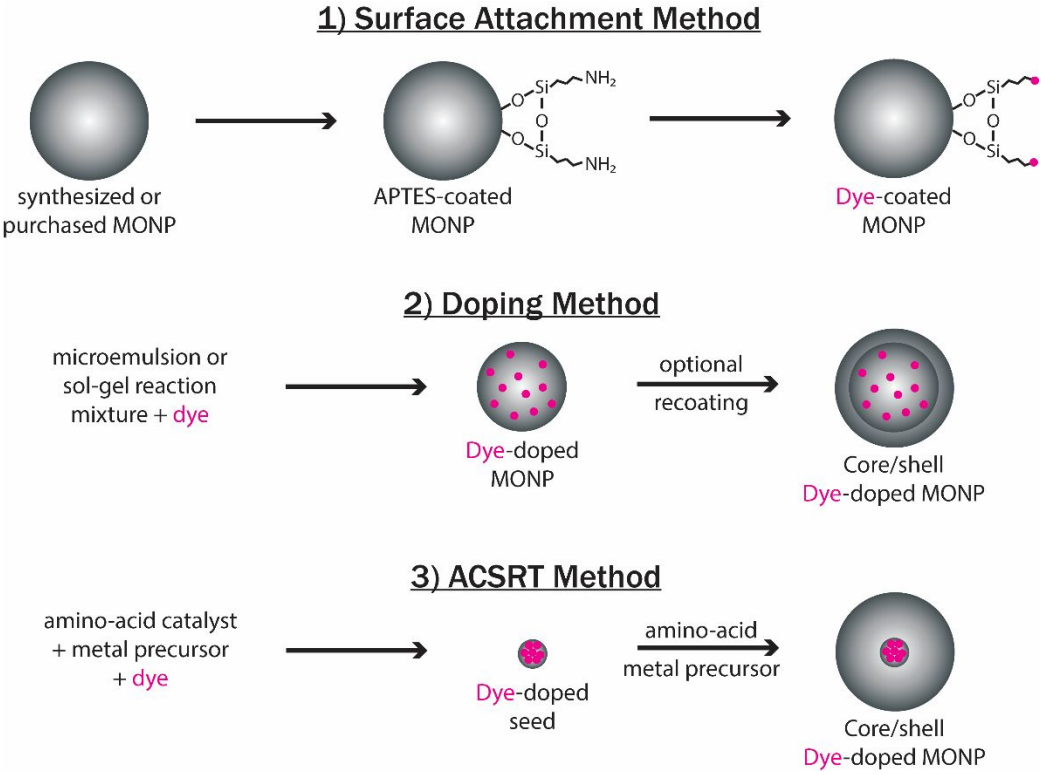

Figure 1. Synthetic techniques used to prepare fluorescent dye-labeled MONPs.

In addition to the dye incorporation method, the dye itself can affect MONP properties and detection. Multiple classes of fluorescent dyes have been employed in MONP labeling, most notably fluoresceins[11,57,60,61], rhodamines[55–57], and perylenes[50,62,63]. Each dye has a different molecular size, charge, and fluorescence spectrum, all of which hold relevance to the properties and detection of the labeled MONP. The optical properties of several common fluorescent dyes have been summarized by Resch-Genger et al.[64]. Photostability varies between dyes, and the chosen dye must remain stable throughout the duration of a study[50,57]. Temperature stability is also important to consider, as it can limit the MONP crystal structures that are able to be formed after the dye has been incorporated. For example, rutile TiO_2 could not be formed using the embedded dye synthetic strategies while keeping the dye intact, as the heat treatments required to

form the rutile structure occur at temperatures much higher than the 200-300°C required to degrade the dye[65,66].

Fluorescently-labeled MONPs have been used to study MONP behavior in a variety of complex systems, including activated sludge biomass[54,55], skin cells and collagens[59,67], and HeLa cells[50,62,68,69]. The most common techniques for visualization and quantification of dye-labeled MONPs are fluorescence spectrophotometry[52,55,60], fluorescence microscopy[50,54,61,63], and confocal microscopy[11,50,56,62]. In one notable study by Xia et al., fluorescent labels were attached to ZnO, CeO_2, and TiO_2 NP surfaces in order to study the subcellular localization of MONPs using confocal microscopy[11]. The FITC-labeled CeO_2 and TiO_2 NPs could be visualized in the caveolae of bronchial epithelial cells and the lysosomes of macrophage cells, despite neither particle type inducing toxic effects to the cells. For ZnO NPs, the FITC-labeled particles could be observed in the caveolae of the bronchial epithelial cells, but not in the lysosomes of macrophage cells, despite inducing toxic effects in both cell types. However, clumping of the macrophage lysosomes was apparent after exposure to ZnO NPs, and Zn^{2+} ions could be visualized in the lysosomes through the use of the Zn^{2+}-sensitive Newport Green indicator, indicating that any ZnO NPs taken up into the lysosomes were likely dissolving and losing the FITC label. Experiments were also performed using Zn^{2+} added as $ZnSO_4$, which showed Zn^{2+} localization within the same compartments as Zn^{2+} added as ZnO NPs. One major drawback of this use of fluorescent dye labeling is that it is impossible to discern the Zn^{2+} that was taken up as ions that had been released into cell media through dissolution, from the Zn^{2+} that was released from the ZnO NPs as they dissolved within the compartment of interest. It is possible that ZnO NPs synthesized using a core/shell synthetic strategy could maintain the fluorescent label long enough to be visible even as they become partially dissolved. Additionally, while this study was

rigorous in the inclusion of free FITC controls and $ZnSO_4$ experiments, there was no comparison of the dissolution rates or surface chemistry of the FITC-labeled MONPs to their unlabeled counterparts. This is especially important when considering that the FITC label was attached to the MONP surfaces through silane linkages, introducing new inorganic and organic components to the surface of the particles that could affect interactions with the surrounding media and tissue. Despite these limitations, this study provides a useful example of the potential of fluorescent dye labeling methods to help elucidate complex toxicological mechanisms.

The primary disadvantage of fluorescent labeling is the relatively high limit of detection provided by the method. Reported limits of detection are as low as 26 μg/L in distilled water[52], but as sample complexity increases, autofluorescence of the background can increase the limit of detection to 77 μg/L in seawater[52] and 500 μg/L in synthetic wastewater[55]. Limits have been reported as high as 5 mg/L[60], and in each case the detection limits can be expected to increase with exposure time due to dye release and photobleaching[70]. Light penetration is limited in intact tissues, which may need to be sliced prior to imaging[70]. The fluorescent label also limits the use of other analytical assays to those that do not have an absorption band overlap with the dye. For example, the silicomolybdate titration for dissolved silica species[71] and several colorimetric assays for reactive oxygen species production[21] cannot be used on fluorescently-labeled MONPs. Additionally, some dyes may be degraded *in vivo*, either through exposure to the acidic environments present in some subcellular compartments, or through enzyme-catalyzed degradation processes[11,72].

However, fluorescence labeling has several major benefits. The preparation of dye-labeled MONPs and the corresponding sample analysis have been consistently reported as less expensive when compared to other labeling methods[60,64] Tools for automating data analysis have also been

developed, including the Particle_in_Cell-3D tool for confocal microscopy images that allows researchers to make rapid comparisons of cellular uptake[62]. Overall, the wide variety of synthetic methods and characterization described in the literature, as well as the commercial availability of fluorescent dyes and dye-labeled MONPs, make this labeling technique one of the most facile to apply.

Radioactive Isotope Labels

Another MONP labeling technique is the assimilation of a radioactive isotope. A summary of radioisotopes used in the study of MONP transport and toxicity is included in Table 2. The three most common methods of producing radiolabeled MONPs are neutron activation, ion bombardment from a cyclotron source, and the use of radioactive precursors. These are summarized in Figure 2. It should be noted that silicon and aluminum do not have useable radioisotopes that can be prepared through direct activation from neutron or ion bombardment[73]. These MONPs can instead be labeled through the activation of ^{18}O to form ^{18}F [74], through ^{7}Be-recoil labeling[75], or through the addition of another material through doping or core/shell methods[60,76–78].

Table 2. Radioisotopes used in study of MONPs.

Radioisotope	Production Method	Half-Life	Radioactivity of MONPs, MBq/mg	Detection Method	Ref.
SiO_2					
^{7}Be	cyclotron, recoil	53.29 d	1	γ-spectrometry	75
^{14}C	^{14}C precursor	5730 yr	8.5×10^{-6}	accelerator mass spectrometry	76
^{56}Co	^{56}Co precursor	77.26 d	1.28	γ-spectrometry	77
^{110m}Ag	^{110m}Ag precursor	249.8 d	9.48×10^{-4}	γ-spectrometry	60
^{198}Au	neutron activation	2.69 d [79]	16.3	γ-spectrometry	78
TiO_2					
^{7}Be	cyclotron, recoil	53.29 d	0.30	γ-spectrometry	80
^{48}V	ion bombardment	15.97 d	0.071	γ-spectrometry	81
^{48}V	ion bombardment	15.97 d	1	γ-spectrometry	82
^{48}V	ion bombardment	15.97 d	3.70	γ-spectrometry	80
^{48}V	ion bombardment	15.97 d	1.0 - 2.35	γ-spectrometry	83–85
^{48}V	ion bombardment	15.97 d	not reported	liquid scintillation counting	86
^{18}F	ion bombardment	109.8 min	0.700	PET	87
^{44}Ti	^{44}Ti precursor	60.4 yr	0.01	γ-spectrometry	80
^{45}Ti	^{45}Ti precursor	3.08 h	135	dose calibrator	80

ZnO					
^{65}Zn	neutron activation	244 d	not reported	γ-spectrometry	88
^{65}Zn	^{65}Zn precursor	244 d	not reported	γ-spectrometry	89
^{65}Zn	neutron activation	244 d	not reported	γ-spectrometry	90
FeO_x					
^{55}Fe	^{55}Fe precursor	2.74 yr	not reported	liquid scintillation counting	91
^{59}Fe	neutron activation	44.5 d	not reported	γ-spectrometry	92
^{59}Fe	^{59}Fe precursor	44.5 d	not reported	whole body counting	93
^{56}Co	ion bombardment	77.26 d	0.113	γ-spectrometry	94
^{125}I	^{125}I precursor	59.43 d	1.85	γ-spectrometry, DAR	95
CeO_2					
^{139}Ce	diffusion	137.6 d	1.242	γ-spectrometry	96
^{139}Ce	ion bombardment	137.6 d	0.975	γ-spectrometry	96
^{141}Ce	neutron activation	35.2 d	0.150	γ-spectrometry	97
^{141}Ce	ion bombardment	35.2 d	0.052	γ-spectrometry	98
^{141}Ce	^{141}Ce precursor	35.2 d	0.100	γ-spectrometry	99–101
^{141}Ce	neutron activation	35.2 d	not reported	γ-spectrometry	90
^{18}F	^{18}F precursor	109.8 min	23	PET	102
Al_2O_3					
^{18}F	ion bombardment	109.8 min	2.31	PET	74
^{13}N	ion bombardment	9.97 min	1.85	PET	103

In the case of neutron activation, post-synthesis MONPs are directly activated through exposure to a neutron flux from a reactor source. This allows the study of many commercially available MONPs, with the exception of TiO_2 NPs due to the lack of appropriate products formed by Ti[104]. Some temperature increase of the materials can be expected during irradiation, causing MONP aggregation or the degradation of some surface coatings, but this can be mitigated by minimizing the neutron flux and amount of material being irradiated[97]. Low increases in the specific radiation activity of the MONPs are unlikely to modify the activities and behavior of the MONPs themselves, but increased radiation exposure could have a confounding effect when determining toxicity in some cases[97].

Direct activation from a cyclotron source can also be applied to commercial or synthesized MONPs. Ion bombardment is more likely than neutron activation to alter material properties through sintering and phase transformations, due to high temperature increases from the Coulomb interaction between the ion flux and the lattice[82,105]. For example, the ratio of the rutile crystalline phase to the anatase phase present in TiO_2 NPs has been shown to increase after

irradiation under certain high activity conditions, a structural transformation that typically occurs above 650°C[97,105]. Holzwarth et al. have shown that thin layers of TiO_2 NPs exposed to protons at energies of 23.5 MeV with a beam current of 5-10 μA will achieve a useful level of radioactivity for detection, without undergoing any thermally-caused changes to the NPs[105]. Cyclotron irradiation can be used to produce positron emitting MONPs labeled with ^{18}F for any material that can be enriched with ^{18}O [74,87]. These labeled materials can be imaged in real-time 3D using positron emission tomography (PET). However, the short half-life of ^{18}F (109.8 min) makes this technique inappropriate for long term-studies. Cyclotron sources are also used for recoil labeling, in which MONPs are irradiated in a mixture with ^{7}Be-forming lithium compounds[75,80]. The ^{7}Be produced is at a high enough energy to become implanted in the MONP structure.

If no cyclotron or nuclear reactor is accessible, a radioactive precursor can be used to label MONPs. This can be accomplished through the use of a radioactive precursor in synthetic procedures, giving researchers more control over MONP properties than direct activation. It can also be used in a low-temperature diffusion process to label MONPs post-synthesis, allowing commonly manufactured MONPs like P25 TiO_2 NPs to be radiolabeled without direct activation[80]. Radioactive precursors are highly expensive, and not all radioisotopes are commercially available or easy to produce, limiting the possible applications of these procedures.

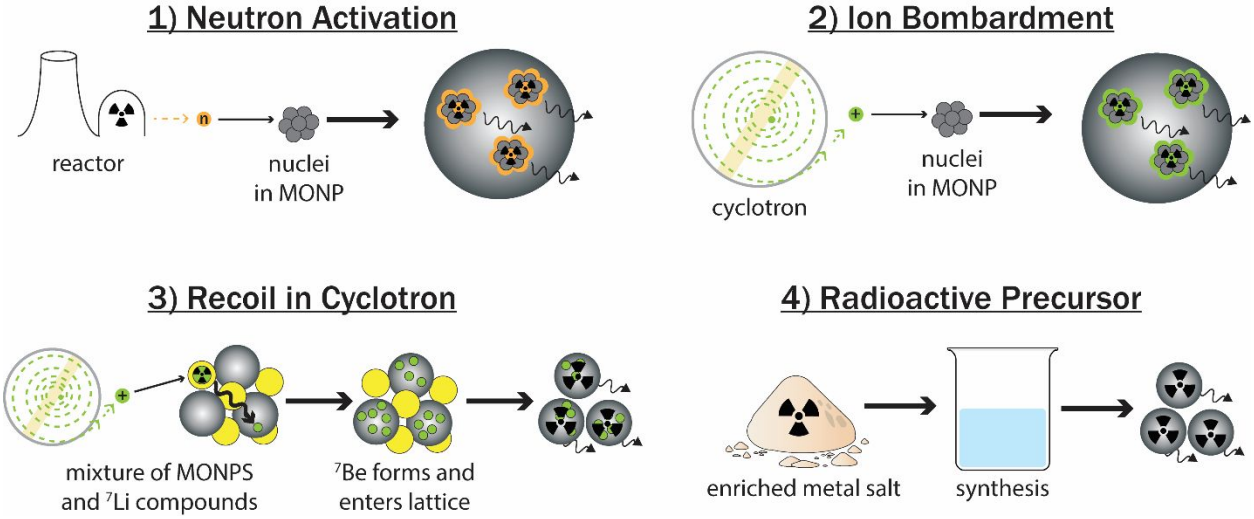

Figure 2. Techniques used to prepare radiolabeled MONPs.

Radiolabeling is especially useful for complex samples that require extensive acid digestion procedures for ICP-MS analysis. Radiolabels can be quantified using several techniques that require limited sample preparation. Scintillation counting allows for the radioactivity of multiple isotopes to be quantified within a single sample through the reaction of the emitted radioactive particles with a fluorescent material (the "scintillator"), creating pulses of light at wavelengths specific to the energy of the emitted particle. This is applicable to α-, β-, and γ-emitting radioisotopes. The quantification of γ-emitting radiolabels can also be achieved through γ-spectrometry using either a scintillation counting detector, or a detector composed of a semiconductive material, in which the emitted radiation causes the promotion of electrons to the conduction band. Ultimately, the limit of detection for a radiolabeled MONP will depend on the resolution and detection efficiency of the detector, the potential interferences from the sample matrix interacting with the emitted particles, and the radioactivity of the prepared MONPs[106]. The resulting radioactivities of labeled MONPs prepared for various studies of behavior and

toxicity have been included in Table 2 to provide a relative comparison of the radioactivity imparted by different radiolabeling strategies.

These advantages related to limited sample preparation have made radiolabeling especially useful for biological studies. Kreyling et al. employed ^{48}V-labeled TiO_2 NPs ([^{48}V]TiO_2 NPs) in a series of three studies to compare the biodistribution and biokinetics of TiO_2 NPs (given to) rats through three different exposure pathways: intravenous, oral, and inhalation[83–85]. Interestingly, the amount of [^{48}V]TiO_2 NPs retained in the syringes used for NP application in each study varied considerably across samples, and up to 50% of the nominal dose was found to be retained in the syringes. The actual applied dose was able to be quantified by directly measuring the amount of [^{48}V]TiO_2 NPs remaining in the syringe using γ-spectrometry, which does not require any rinsing or further treatment of the syringes that could confound the measurement. This determination of the actual applied dose, in addition to the quantification of [^{48}V]TiO_2 NPs across the entire rat body and in excretions, allowed for a complete mass balance to be developed. The resulting values were also corrected for the potential release of the ^{48}V label through the use of complementary studies that identified differences in behavior between ionic and particulate ^{48}V. These studies used a highly quantitative approach made possible through radiolabeling to show that intravenous injection of NPs does not result in the same biological behavior as other routes of exposure, and should not be used as a surrogate experimental method.

Radiolabeling methods have several limitations, including the requirement of access to controlled laboratory space and specialized equipment. The safety precautions that must be taken in handling radioactive materials often limit characterization of labeled MONPs to techniques that require a very small amount of material. In some cases, the specific activity level of labeled

materials may be high enough to influence toxicity toward an organism through exposure to radiation; it is therefore recommended that additional toxicological studies are performed in tandem with unlabeled materials when the specific activities and NP doses are high. Finally, radiolabeling techniques are expensive. Synthetic costs using radioactive precursors were reported as fifteen times higher than the cost of fluorescence labeling for SiO_2 NPs[60].

The primary advantage of radiolabeling is that it provides the lowest detection limits of any labeling method with very little sample preparation required for analysis. Detection limits depend on the specific activities of the radiolabeled MONPs and the type of detector used, but these values typically fall in the range of pg/L to ng/L. Radiolabels can be directly applied to commercial MONPs in addition to lab-synthesized MONPs, allowing researchers to study the most environmentally relevant materials. Quantification can be achieved along with real-time imaging, providing important information about the mechanisms of MONP uptake, metabolism, and toxicity.

Stable Isotope Labels

In stable isotopic labeling, MONPs are labeled through enrichment with a stable isotope of the relevant metal that occurs at a low abundance in the environment. Many stable isotopes have been successfully employed in the study of MONPs, as summarized in Table 3. The preparation of MONPs enriched with a stable isotope is achieved through synthesis with an enriched precursor material. Enriched precursors are commercially available as soluble salt complexes, solid metals, or solid metal oxides. In the cases of enriched metals and metal oxides, the material must be broken down using acid digestion prior to MONP synthesis. Once a soluble metal isotope solution is achieved there is no limit to the customization (e.g. shape, size, crystal structure, surface coating) that can be applied to an isotopically-labeled MONP. The main

limitation inherent in the preparation of MONPs labeled with stable isotopes is that commonly manufactured MONPs cannot be effectively labeled with stable isotopes post-synthesis.

MONPs labeled with stable isotopes are most often quantified using ICP-MS, which may also be coupled to FFF or other sample fractionation techniques. The limits of detection for these studies will depend on the relative abundance of the labeling isotope, the presence of any interfering complexes in the sample matrix, and the resolving precision of the instrumentation. To identify the amount of the labeling isotope that corresponds to the MONPs, the concentration of the isotope in the background matrix must be determined and subtracted. This can be achieved by measuring the labeling isotope directly, or by measuring another isotope of the same metal and using the natural ratio of the isotopes to correct in calculations. In cases where the sample matrix is heterogeneous, it may be preferable to measure a non-labeling isotope in each individual sample, as opposed to measuring the labeling isotope in a smaller set of "background" samples. Using labeling isotopes with lower abundance will increase detection sensitivity, but these precursors are more expensive. Isotopic labeling studies also require that attention is paid to potential isobaric and polyatomic interferences that affect the determination of the isotopic ratio within a sample. For example, matrices high in sulfates can interfere with the detection of multiple isotopes of Ti, while Ce measurements are impacted by the presence of neodymium[45,107,108]. Polyatomic interferences for each element have been summarized by May and Wiedmeyer[109].

Quantifying isotopic ratios within a sample requires high instrumental precision in resolving peaks between two adjacent isotopes. Isotopically-labeled MONPs can be quantified at environmentally relevant concentrations using conventional quadrupole ICP-MS instruments alone, but sensitivity can be increased even further through the use of high resolution multi-

collector ICP-MS (MC-ICP-MS) instruments[108,110]. MC-ICP-MS instruments are much more expensive than conventional ICP-MS instruments, but may be especially useful in cases where organisms are chronically exposed to very low doses of MONPs.

In addition to quantification using ICP-MS, isotopically-labeled MONPs can be visualized within a sample using time-of-flight secondary ion mass spectrometry (ToF-SIMS)[111]. In a study of ZnO NP uptake and toxicity in HaCaT cells, the luminescence of ZnO NPs and the use of a stable ^{68}Zn label allowed for both confocal laser scanning microscopy (CLSM) and ToF-SIMS to be used within the same study. ToF-SIMS provided a two dimensional image free from background interference, which was then compared to the three dimensional CLSM images. It was determined that Zn^{2+} ions from ZnO NPs are absorbed and transported into the cytoplasm and nuclei, and that the relative amounts of intracellular Ca^{2+} and K^{+} are affected by the ZnO NP dose. Laser ablation ICP-MS (LA-ICP-MS) can also be used for 2D imaging of samples containing isotopically-labeled MONPs. However, this technique offers spatial resolution of only 5-20 μm, while ToF-SIMS can be operated to provide sub 100 nm resolution[70,112].

Stable isotopic tracers are often used in studies of ZnO and CuO NPs, due to the labeling method's effectiveness for MONPs that dissolve throughout the course of the experiment. Ions released directly from the MONPs will still bear the isotopic label and can be quantified using the same methods of analysis used for the MONPs[113]. It is also possible to use more than one stable isotope in the same study to gain a better understanding of the localization of released ions versus the nanomaterial. Laycock et al. used a combination of ^{68}ZnO NPs and $^{64}Zn^{2+}$ ions incubated in soil from 1-12 months to study uptake in earthworms[114]. As the soil incubation time increased, the amount of Zn from all forms increased in the pore water, resulting in higher bioaccumulation efficiencies. There was no discernable difference between the relative amounts

of ^{68}Zn and ^{64}Zn in the different compartments (soil, water, and organism) of the experiment, which supports the hypothesis that the ^{68}Zn was taken up in the ionic form after the ^{68}ZnO NPs dissolved in the soil media. One method to help determine whether this is the case would be to extend an approach developed by Merrifield and Lead, in which multiple isotopic labels were embedded in the same nanoparticle[115]. In this study, a three-layer silver nanoparticle was synthesized with two different stable isotopes labeling the core (^{109}Ag) and the shell (^{107}Ag). These were separated by a layer of gold that was added to prevent core dissolution, ensuring that only the ^{107}Ag from the NP shell would be exposed to organisms in the ionic form. Comparing the concentrations of the two silver isotopes in both the exposed organisms and the media would allow for the determination of the relative contributions of the ionic versus particulate silver. Although this method has only been applied to silver nanoparticles, the same approach could be extended to soluble MONPs like ZnO NPs.

The primary disadvantage of stable isotopic labeling is that the manufactured MONPs that are the most environmentally relevant to study cannot be effectively labeled after purchase. One possible solution to this problem is the use of the "reverse labeling" procedure developed by Croteau et al.[116,117]. In one study, freshwater snails were chronically exposed to ^{65}Cu isotopes until the isotopic ratios within the snail tissues was altered, effectively eliminating the metal background from the experiment[116]. This enabled researchers to measure the uptake of Cu, which naturally primarily contains the isotope ^{63}Cu, from particles that had been collected from a river impacted by acid mine drainage. The naturally aged complex colloids composed of a mixture of Al and Fe oxides with sorbed Cu were able to be tested directly on the organisms. A similar approach was used to study Zn uptake in snails from natural particles collected from two acid mine drainage impacted rivers[117]. The authors were able to show that a higher strength of Zn

sorption to the collected particles resulted in lower assimilation within the organisms. This reverse labeling technique is effective for biological studies involving essential elements like Zn, Cu, and Fe, which will be easily assimilated into the organism. It remains to be seen whether this approach can be extended to other MONPs comprised of metals that are not essential elements. Another potential drawback is that the media that the experiment is performed in must be free of the background metal. Thus, the reverse labeling approach would be difficult to apply in experiments requiring the use of complex natural media. This issue could be mitigated through control experiments identifying differences in the fate and uptake of the element of interest from the media alone when compared to the MONPs.

Despite this drawback, there are major advantages to stable isotopic labeling. MONPs can be detected at very low, environmentally relevant concentrations. Stable isotope labels are the most enduring of any technique, are measurable even in ions released from dissolution, and do not have the equipment and safety limitations of radioisotopes. Additionally, there is likely to be no impact on MONP properties, although extra care must be taken not to introduce artefacts during the sample preparation required for quantification.

Table 3. Stable isotopes used in study of MONPs.

Stable Isotope (% Rel. Abundance)	MONP Studies Employing Stable Isotope	Reported Limits of Quantification
TiO_2		
^{47}Ti (7.5)	• Bioaccumulation in mussels[118]	8.6 ng/L in mussels[118]
ZnO		
^{64}Zn (48.6)	• Uptake of Zn^{2+} vs ZnO NPs in earthworms using multi-isotope approach[114]	
^{67}Zn (4.1)	• Uptake in snails[119,120] • Uptake in endobenthic organisms[121]	< 15 μg/g in snails[120]

^{68}Zn (18.6)	• Dermal absorption of ZnO NPs from sunscreens in mice and humans[122–126] • Uptake and cytotoxicity to human skin cells[111] • Bioavailability of ZnO NPs vs. bulk Zno vs. Zn^{2+} ions to aquatic organisms[113] • Uptake and elimination for bulk vs. nano-sized ZnO[127]. • Evaluation of cost-effectiveness for Zn isotopic labels[128] • Up take of Zn^{2+} vs ZnO NPs in earthworms using multi-isotope approach[114]	5 ng/g[128] 175 ng/g in blood[123]
CuO ^{65}Cu (30.8)	• Synthesis and detection of spherical and rod-shaped ^{65}CuO NPs[129] • Uptake of CuO NPs vs. Cu^{2+} in freshwater worms from aquatic and sediment exposures[130,131] • Toxicity and bioaccumulation in snails[132]	10 ng/g in snails[129]
FeO_x ^{57}Fe (2.14)	• Exchange of atoms between goethite nanorods and dissolved Fe^{2+} [133,134] • Detection of $^{57}Fe@SiO_2$ NPs in river sediment slurry[135]	7.8 µg/L Fe in river sediment slurry[135]

Dopant and Core/Shell Labeling

The final category of MONP labeling techniques is the use of dopants and core/shell labels. In the case of doping, MONPs are synthesized with another metal that is rare in the samples of interest replacing a fraction of the metal present in the MONP lattice structure. It should be noted that some radiolabels that feature an element not present in the unlabeled MONP, e.g. those prepared through ^{7}Be recoil labeling, are also effectively labeled with a dopant. To prepare dopant-labeled MONPs featuring another nonradioactive label, existing sol-gel synthesis and hydrothermal methods can be altered by adding a soluble salt of the labeling metal to the MONP metal-alkyl precursor solution. The amount of dopant present in the final labeled MONP can be adjusted by altering the stoichiometric ratio of the labeling metal to the primary metal in the solution[136,137]. ICP-MS or ICP-optical emission spectrometry (ICP-OES) can be used to quantify the amount of labeled MONPs through the known ratio of the traceable metal to the MONP

metal. TiO_2 NPs have been doped with La, Ce, Nb, Zr, and Hf to enable detection within complex matrices[86,137,138]. Limits of detection for Ce-doped TiO_2 NPs have been reported as low as 16.8 μg Ce/L using ICP-OES[137]. Only a small fraction of Ti atoms needed to be replaced for this degree of sensitivity: the ratio of Ce to Ti was varied from 0.005 to 0.03 in this study. However, replacing the metal of interest within the MONP lattice with another metal that has a different ionic radius can impact particle properties like the size, specific surface area, crystallinity, and electronic band gap[138,139]. The concentration of the dopant can affect the degree to which the electronic properties are altered[139], with the highest enhancements of the photoactivity of rare earth element doped TiO_2 NPs occurring at dopant concentrations below 1% by weight[140]. Dopants have also been shown to preferentially appear on the surface of the MONPs as opposed to the bulk, where they will interact directly with the surrounding media[137]. Overall, it is important to monitor the electronic and surface properties of dopant-labeled MONPs, as changes to these properties can affect behavior and toxicity in experimental studies[139].

In core/shell labeling, a variety of materials have been incorporated as the MONP labels, as summarized by Figure 3. The label is typically another metallic nanoparticle, which is then coated with the MONP material. One core material that can be used is quantum dots (QDs), which have the useful luminescent properties of a fluorescent dye label with more long-term stability. The QDs most appropriate for MONP labeling applications are typically composed of CdSe or CdTe NPs that range from 1-6 nm in diameter[64]. QDs can be synthesized or commercially purchased and then coated with MONP materials using microemulsion, sol-gel, or amino acid driven synthetic methods. It is important to ensure the shell prevents the release of QDs or the ions present in them, as they will have different behaviors and toxicities when

compared to the MONP-coated QDs[141,142]. In addition to quantification using fluorescence-based techniques, the core materials in QD-labeled MONPs can also be quantified by using ICP-MS. SiO_2-coated CdSe/CdS/ZnS QDs were used to study the potential impacts of oral exposure to SiO_2 NPs in a mouse model, and the known ratio of Cd:Si was used to confirm via ICP-MS that the fluorescent particles imaged in the liver came from the labeled MONPs and not the sample background[56].

Noble metal nanoparticles have also been used for core labeling. SiO_2 NPs have been labeled with an AgNP core, while TiO_2 NPs have been labeled with an AuNP core[60,143]. In the case of AgNP cores, dissolution of the core label can be a concern: Ag^+ ions began to be released from the labeled SiO_2 NPs after 20 days of storage in deionized water[60]. While a variety of synthetic methods for core/shell MONPs featuring noble metal NP cores have been presented, most often these procedures were developed to create MONPs with enhanced catalytic properties and will need to be adjusted to mitigate these effects[144–147]. Once the MONP shell is deposited onto the noble metal core, solvothermal treatments may be necessary to achieve the MONP crystal structure desired. Here, it is necessary to take steps to prevent any thermally-induced structural changes to the AuNP or AgNP core, which for rutile TiO_2 can be achieved by adding an additional SiO_2 shell that is later removed through etching[144]. ICP-MS is typically used for quantification, resulting in a reported limit of detection of 24 μg/L for Ag@SiO_2 NPs[60]. Au@TiO_2 NPs have been accurately quantified at levels of 1.5 μg Ti/L in deionized water using ICP-MS and 750 μg Ti/L in a river water-sunscreen mixture using ICP-OES[143]. Single particle ICP-MS can also be applied as a characterization tool and quantification strategy. In addition, Au@TiO_2 NPs have been quantified in activated sludge using instrumental neutron activation analysis (INAA), with reported limits of detection and quantification of 16.8 mg Ti/kg sludge

and 25.8 mg Ti/kg sludge, respectively[143]. The core/shell labeling approach allows INAA quantification to be extended beyond facilities with a reactor on-site, as the experiment can be performed prior to irradiation and then samples can be transported for analysis.

Finally, one novel and interesting core-labeling method is the encapsulation of DNA barcodes within a SiO_2 shell. To achieve this, SiO_2 NPs are prepared with positively-charged functional groups on the surface. DNA is then adsorbed onto the positively-charged SiO_2 surface, and encapsulated in an SiO_2 shell using a sol-gel process[148]. The encapsulated DNA has been shown to be stable in the presence of ROS and in temperatures up to 120°C. The DNA can be released using an etching agent, and quantified using quantitative polymerase chain reaction (qPCR) methods at concentrations as low as 100 ng Si/L[149]. This technique has been used to study SiO_2 colloid transport within wastewater treatment systems, and the transfer of SiO_2 colloids between trophic levels[149,150]. When digital particle PCR (dpPCR) is used for quantification, individual SiO_2 NPs can be detected and counted, resulting in a limit of detection of approximately one particle per μL solution[151].

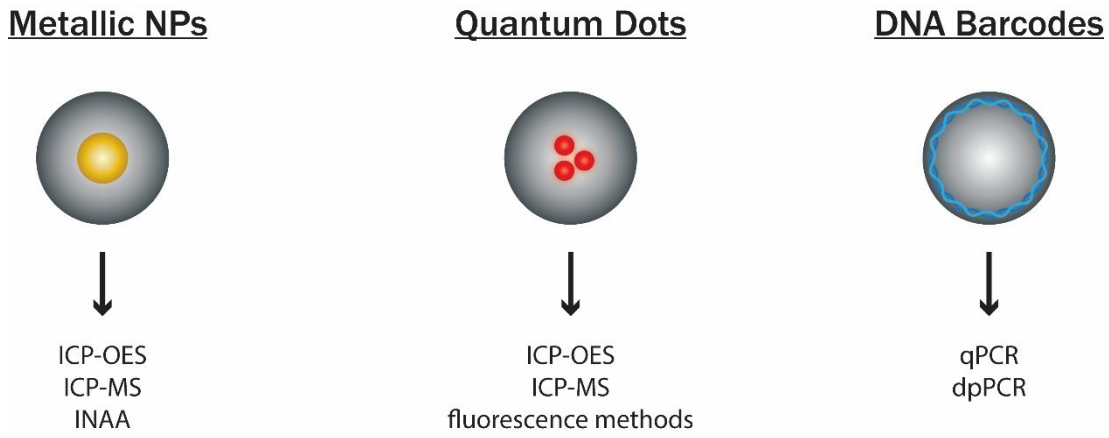

Figure 3. Label materials and quantification techniques used for core-labeling strategies.

Doping and core/shell labeling techniques provide unique advantages and disadvantages. Metallic labels are more stable than fluorescent dyes, but can potentially be released as ions in

the cases of dopants on the MONP surface, or core labels comprised of materials susceptible to dissolution. With the exception of DNA barcode labels, dopant and core/shell labeling techniques are more inexpensive than isotopic labeling strategies, while some of the same quantification techniques (ICP-MS, INAA) can be employed. Some core/shell systems are also compatible with sp-ICP-MS techniques, which can provide number concentrations and size distributions for the core particle within a complex sample. The primary disadvantages are that these techniques cannot be applied directly to commercially available nanoparticles, and that some properties of the unlabeled MONP may be affected. These include photocatalytic activity for both dopants and core labels, and density for core labels.

Properties and Characterization of Labeled MONPs

A critical step in employing any labeling method is the proper characterization of the resulting labeled MONPs and comparison to their unlabeled counterparts. Without this characterization, it remains uncertain whether the labeled MONP's behavior determined within a study can be truly representative of the MONP. The MONP properties that could potentially be altered through the incorporation of a label, resulting in changes to behavior, are discussed in detail in this section and summarized in Table 4. Table 4 also lists some of the most common characterization techniques used to probe these properties. It is important to note that this list is not exhaustive, and that new techniques will continue to be developed after the publication of this article.

The defining property of nanomaterials that has given rise to concern about their potential environmental implications is their size. Nanoparticles of different sizes exhibit differences in cellular uptake and localization, as well as differences in the overall toxicity to a variety of organisms[152–155]. Isotopic labeling featuring the use of an enriched precursor is unlikely to alter

MONP size, since identical synthetic procedures can be used for both the labeled and unlabeled MONP. However, synthetic procedures for labeling using dopants, core/shell structures, and fluorescent dyes will need to be optimized to ensure that the size of the labeled MONP corresponds to the size of interest for the unlabeled MONP. In the case of direct radioactivation, exposure to extreme temperatures during irradiation could potentially impact the MONP structure and alter the size. Primary particle size can be measured using electron microscopy techniques. The hydrodynamic diameter, which takes into account MONP agglomeration and solvation, can be determined using dynamic light scattering (DLS) or nanoparticle tracking analysis (NTA)[156].

In some cases, the size of the individual crystallites that compose MONPs may differ from the primary particle size. Crystallite size can be measured using x-ray diffraction (XRD) or TEM analysis. The crystal structure of the MONPs can also be measured using XRD or determined using selected area electron diffraction (SAED) performed within TEM analysis. Differences in the crystallite size or crystal structure between the labeled and unlabeled MONPs will impact the surface area and photocatalytic activity of MONPs[157,158]. Characterizing these differences is especially relevant for doped MONPs, where changes in the elements present in the lattice structure give rise to differences in atomic spacing that can impact crystallite size. Alterations to the crystalline properties are also likely to occur for labeling techniques that expose the MONPs to different temperature treatments than their unlabeled counterparts. This includes labels like fluorescent dyes that may require differences in the synthetic temperatures to prevent dye degradation, and direct radioactivation techniques that may expose MONPs to high temperatures.

Closely related to size is MONP surface area, which can affect toxicity through its relationship to photocatalytic activity, ROS generation, and dissolution kinetics[159,160]. The

specific surface area (SSA) is commonly determined using Brauner-Emmett-Teller (BET) analysis, which uses the measurement of the physical adsorption of small nonreactive gas molecules to a dry nanopowder, allowing for the porosity of the particles to be included. Changes to this parameter would most likely be brought about by dopant, fluorescent dye, and core/shell labels, which are the most likely to impact the porosity of the MONPs due to the incorporation of labeling compounds that differ in size and properties from the MONP materials. The SSA measured via BET analysis does not take into account the agglomeration state of the MONPs once they are in solution. Surface area can also be estimated using size measurements from DLS or electron microscopy and the density of the bulk material[161]. For core/shell-labeled MONPs, the ratio of the core and shell should be tuned to maximize similarities between the primary particle size, surface area, and density of the labeled and unlabeled MONPs while maintaining a large enough core size to achieve sufficient detection sensitivity. Density can be estimated from size measurements, or directly compared using differential sedimentation or 2D analytical ultracentrifugation[162,163].

Another group of properties that must be examined when labeling techniques are employed are those that comprise MONP surface chemistry. This includes the functionalization of MONPs with a stabilizing ligand, the surface charge, and the relative hydrophobicity or hydrophilicity of the surface. These surface properties have an important impact on the bioavailability and toxicity of nanomaterials due to the impact on aggregation state, dissolution rate, adsorption of natural organic matter or other biomolecules (corona formation), and interactions with cells and organisms[155,164–167]. A variety of surface coatings are used on MONPs to impart stability through electrostatic or steric repulsion, to enhance dispersion within an MONP-enabled product, or to control the MONP reactivity. For some MONP labeling strategies, the incorporation of a

functionalized surface coating will not be possible. This includes the surface attachment of fluorescent dyes to MONPs, which can prevent or limit another functional ligand from being attached to the surface. Additionally, direct activation techniques for radiolabeling are generally not applied to MONPs with a surface coating, as the coating is likely to be altered and could also impact the amount of radioactivity imparted to the metal oxide. Doped MONPs may have differences in the total coverage of a surface coating due to differences in lattice spacing and binding behavior between the metal oxide and the dopant label.

In addition to coatings applied to MONPs during synthesis, coatings of proteins or organic acids that form from the surrounding media can also control environmental behavior. It is well established that the adsorption of natural organic matter and other biomolecules and proteins to MONP surfaces are a function of the properties of the particles (surface charge, crystal structure, morphology, engineered coatings) and the suspending matrix[168–170]. Furthermore, the resulting "eco" or "bio" coronas are a strong determinant of the fate, transport and toxicity of these materials[170]. As such, any aspect of a given labeling technique that would alter the nature of engineered or acquired coatings has the potential to impact behavior in complex matrices and must be examined. A variety of analytical strategies are available for the characterization of both intentionally applied and incidentally adsorbed NP coatings, as reviewed by Louie et al.[165]. Commonly utilized techniques include x-ray photoelectron spectroscopy (XPS), thermogravimetric analysis (TGA), and attenuated total reflectance Fourier transform infrared spectroscopy (ATR-FTIR)[171–173]. Techniques for the characterization of NP protein coronas specifically have been reviewed by Capriotti et al.: commonly utilized techniques include capillary electrophoresis (CE) and size exclusion chromatography (SEC)[174].

In the current body of literature, ζ-potential (a surrogate for surface charge) is often the primary characterization performed to compare the surfaces of labeled and unlabeled MONPs, with the implication that a consistent ζ-potential will result in consistent transport behavior. Since ζ-potential measurements depend on a combination of the nanomaterial, solution, and instrumentation, information about each of these relevant parameters must also be reported[175]. It is important to recognize that differences in the steric stability or hydrophobic/hydrophilic properties of a labeled MONP can still be present even when the ζ-potential is unchanged by the label. DLS can be used to determine the critical coagulation concentrations and aggregation behavior of MONPs in different aqueous media as a way to identify differences in electrostatic and steric stability between labeled and unlabeled MONPs. The adsorption of dyes like Rose Bengal and Nile Blue can be used to characterize the hydrophobic/hydrophilic surface properties of MONPs[176–178]. Comparing the deposition behavior of labeled and unlabeled MONPs in a controlled system increases confidence that the labeled MONPs will be an equivalent surrogate in a complex transport study. Deposition behavior can be studied using quartz crystal microbalance (QCM), column filtration studies, or surface affinity functional assays[179–182].

The surface properties of MONPs are most likely to be affected by labels that appear directly on the surface of the MONP, like dopants and surface-attached fluorescent dyes. The likelihood of the label to interact directly with the surrounding media can also be evaluated separately from other aspects of surface chemistry. For metal labels used as dopants or in core labels, XPS analysis can be used to determine the elemental composition of the surface of the labeled MONP, which can then be compared to the bulk composition measured by another method (e.g. ICP-OES, ICP-MS, INAA, or EDS/EDX). Determining the effects of changing solvents on the optical or fluorescent properties of the label within the MONP is another useful indicator of label

impact: a greater solvatochromic shift indicates more exposure of the fluorescent dye to the outside medium, and a greater probability that the dye could influence behavior[50,57].

There are several MONP characteristics that are directly related to the potential for toxicity. First, the overlap of the band gap energy of an MONP with the energy potentials of key cellular redox processes has been shown to be a strong predictor of toxicity for low solubility MONPs[183]. Band gap energies can be determined using diffuse reflectance UV-Vis spectroscopy[183]. For ZnO and CuO NPs, particle dissolution and release of ions is the primary mechanism of toxicity, making the label impact on dissolution behavior important to consider. Dissolution can be quantified by exposing MONPs to the media of interest, separating MONPs from released ions through filtration or centrifugation, and measuring the concentration of the metal ions using ICP-OES or ICP-MS techniques. Surface redox reactivity can be measured using a colorimetric assay for methylene blue reduction developed by Corredor et al.[184], and has been shown to correlate to antimicrobial activity for CuO NPs[185]. Finally, a variety of colorimetric assays exist for the determination of ROS production by NPs, as summarized in reports by Djurišić et al. and Crandon[21,178]. Most notably, 2′7′-dichlorofluorescein diacetate (DCFH-DA) is a commonly used nonspecific probe that applies to both intracellular and acellular ROS generation[21,178,186]. Here, exposure to ROS causes the oxidative conversion of DCFH to the fluorescent product DCF, which can be easily measured using fluorescence spectrometry and converted to equivalents of hydrogen peroxide using a standard curve. To study ROS generation under irradiation for photocatalytically active materials like TiO_2, a procedure has been developed that measures the conversion of fluorescein to non-fluorescent products[187]. Electronic properties like the band gap energy or the potential to generate ROS are most likely to be affected by metallic dopant and core/shell labels, which can increase the formation of oxygen vacancies on the MONP surface or

participate directly in charge transfer and subsequent band gap narrowing with the MONP material [188–191]. Core labels composed of plasmonic NPs can also affect the electronic properties by creating intense electric field "hot spots" on the MONP surface, with a much greater potential to generate electron-hole pairs in photocatalysis than the rest of the MONP surface[188,192].

Proper characterization of a label's impact to MONP properties helps ensure that the overall transport or toxicity is not affected. Additionally, if differences in the studied behavior for labeled versus unlabeled MONPs are discovered, rigorous characterization of the individual properties of the MONP could assist in revealing mechanistic insights into the behavior.

Table 4. MONP Properties and Characterization Techniques

MONP Property	Commonly Utilized Characterization Methods
Size	SEM/TEM, DLS, NTA, FFF, sp-ICPMS
Crystallite Size	XRD, TEM
Crystal Structure	XRD, SAED within TEM analysis
Surface Area	BET, Calculations from size
Presence of Surface Coatings and Coronas	TGA, XPS, ATR-FTIR, CE, SEC
Surface Charge	ζ-potential, Surface charge titration
CCC, Aggregation Behavior	DLS, NTA
Deposition Behavior	QCM, column filtration studies, surface affinity functional assay
Density	Differential sedimentation, 2D analytical ultracentrifugation
Hydrophobicity/Hydrophilicity	Adsorption of rose bengal and nile blue dyes
Band Gap Energy	Diffuse reflectance UV-Vis
Dissolution	ICP-OES, ICP-MS
Photocatalytic Activity	Methylene blue dye degradation under UV exposure
Surface Redox Reactivity	Methylene blue reduction assay
ROS Generation	Colorimetric assays using dye indicators (e.g. DCFH-DA)

In addition to characterization techniques that determine whether the label has impacted particle properties, characterization should also include factors related to the detection sensitivity and stability of the labeled MONPs. For MONPs labeled with a stable isotope or another metal, detection sensitivity is controlled by the elemental or isotopic ratios of the labeled MONPs, which can be measured using ICP-MS. For fluorescent MONPs with dyes or QDs incorporated as labels, the fluorescence quantum yield should be determined using fluorescence spectrometry. The radioactivity of MONPs labeled with radioisotopes can be measured using scintillation

counting or γ-spectrometry. The stability of the label should be evaluated for the relevant media, temperatures, and time-scales of the experiment, to ensure that the label will not be released. Along with this information, the limit of detection (LOD) and limit of quantification (LOQ) should be determined and reported for the media of interest. Numerous efforts have been made within the nanotoxicology community for more complete characterization of all NPs used in studies evaluating toxicity and exposure[193,194]. In the case of labeled MONPs, it is especially vital that the property-activity relationships determined through experimental work are inferred based on the true properties of the material, and not confounded by the impact of the label.

Evaluation of Labeling Strategies

Each labeling technique has several advantages and limitations. The decision of which labeling strategy to use will be based on balancing the detection sensitivity, label stability, cost and equipment requirements, label effects on MONP properties, and ease of labeling and quantification. Table 5 provides a summary of these qualities for each labeling approach.

In terms of detection sensitivity, radiolabeling methods are the most sensitive of any technique, offering detection limits as low as pg/L even in complex matrices like mouse tissues. Fluorescent dyes offer the lowest amount of detection sensitivity, often with detection limits higher than environmentally relevant doses. Sensitivity can be decreased even further in matrices that prevent the luminescence of the particles from reaching a detector. Stable isotopes, dopants, and core/shell labeling techniques fall into the detection limit range of ng/L-µg/L, allowing for sensitive detection with a variety of quantification techniques.

Also relevant to detection sensitivity is the stability of the label, both over time and in a variety of matrices. Here, stable isotope labels offer superior stability. They do not degrade over time, and are released from the labeled MONP only as the free ions that would be released

through dissolution in an unlabeled particle. These ions can still be detected against a background. For radioisotopes, there exists a wide range of half-lives, and it is important to ensure that the radioactive decay will still allow for the required detection limits to be achieved at the end of the experiment. In addition, small amounts of the radiolabel may diffuse to the surface and be released from the MONP[83–85]. For fluorescent dye labels, the label has been consistently shown to leach from particles over time. Some core labels like AgNPs and QDs may also leach toxic ions that impact study results. The stability of dopant labels under biological conditions has not been adequately investigated. Coating the doped MONPs with a layer of the undoped metal oxide may assist in preserving the dopant labels. In each case, it is necessary to perform experiments testing label stability in the matrix of interest. To adjust for label release, controls should be performed to determine differences in behavior between the free label and labeled MONP. In terms of temperature stability, organic materials like fluorescent dyes and DNA barcodes are the most likely to degrade. It is unlikely that these types of labeled particles can be heat treated to form all MONP crystalline structures without damaging the integrity of the label. If these materials are not adequately protected within the MONP shell, enzymes and ROS produced by organisms may also degrade the labels.

Cost and equipment requirements can be a limiting factor in choosing a labeling strategy. Isotopic labeling techniques are the most expensive, as isotopically-enriched reagents and direct radioactivation techniques are costly. The cost of the enriched reagent material necessary to produce 100 mg of ZnO NPs ranges from $4000 to $35000 for the stable isotopes summarized in Table 3[128]. In the case of radiolabeling, there is not only specialized equipment required for the production and quantification of the MONPs; there are also equipment requirements and costs associated with the safe use and disposal of radioactive materials. Fluorescent dyes are by far the

most inexpensive label to incorporate and quantify. In one comparative study, fluorescently-labeled SiO_2 NPs cost 2.7 times less to synthesize than AgNP core-labeled NPs, and 15 times less than radioactive AgNP core-labeled NPs[60]. Quantification of the fluorescent NPs cost 7 times less than the AgNP core-labeled NPs, and 5.2 times less than the radioactive AgNP core-labeled NPs[60].

The applicability of the label to a specific type of MONP is one aspect that may be the deciding factor in choosing a specific labeling method for a given study. Some labels, such as NP cores or dopants, cannot be applied to pre-synthesized, commercially-available MONPs. These commercial MONPs are utilized in large quantities, and as such the potential environmental impact is of interest to researchers. Direct radio-activation is the best labeling option for pre-synthesized MONPs that do not contain organic stabilizing ligands that could degrade during neutron or ion bombardment. While diffusion labeling using isotopes and the surface attachment of fluorescent dyes also apply to commercial MONPs, the stability and detection sensitivity offered by these labels is much lower. Other MONP labeling techniques are not appropriate for labeling highly soluble MONPs. These include core/shell, dopant, and fluorescent dye labels.

The potential effects of labels on key MONP properties have been discussed in detail in the previous section. To summarize, MONPs labeled with stable isotopes are the least likely to have properties impacted due to being elementally and structurally identical to the unlabeled MONP. MONP surface properties are most likely to be affected by dopant labels and by fluorescent dyes that have been attached to the MONP post-synthesis. Surface chemistry will affect aggregation behavior, the formation of protein coronas, and interactions with biomass. Photocatalytic activity and other electronic properties are most likely to be impacted by the incorporation of other metals, especially plasmonic metals like gold and silver, into the MONP as cores or dopants. The

electronic properties of the MONP control the potential to generate ROS and impart toxicity for MONPs where dissolution is not the primary mechanism of toxicity. The dopant concentration or core size should be optimized to limit these effects.

To provide guidance on how to choose and employ a specific labeling technique for a given study, two case studies will now be explored. First, we consider a hypothetical 90 day study examining TiO_2 NP distribution and toxicity within 60 L mesocosms containing multiple trophic levels of organisms. A real-world example of this type of mesocosm study has been performed by Bour et al[195]. For this hypothetical study of TiO_2 NPs, it can be expected that background titanium will be present in the water, sediment, and organisms contained in the mesocosms. The use of a label will enhance detection sensitivity while also limiting the impact of heterogeneity in the levels of background titanium within different samples of the same mesocosm compartment. This type of study requires a label that can be produced and used in large quantities, is highly stable over time, and can be easily quantified down to low μg/L concentrations. The limitations on the quantities of radioactive materials that can be handled, as well as the short half-life of many radioisotopes, prohibit the use of radiolabels in this hypothetical study. While stable isotopes offer the stability and detection sensitivity required, the high expense of producing the quantity necessary to evaluate their behavior in multiple mesocosm experiments is undesirable. Fluorescent dyes typically do not provide the detection sensitivity required, and may also be released from the MONP or degraded by photobleaching over the course of the study. A metallic label, used as either a dopant or a core label, is highly stable over time and provides low limits of quantification even in complex media. The cost of producing the dopant or core-labeled MONP is not as high as for isotopic labeling, and multiple TiO_2 crystal structures can be formed. A variety of quantification techniques can also be used, including ICP-OES, ICP-MS, and even

INAA. This provides flexibility that allows samples from compartments that are difficult to prepare for ICP-MS analysis to be quantified by INAA, while samples from compartments with higher concentrations of MONPs can be easily quantified by ICP-OES. The size, surface charge, and aggregation behavior should be compared between the labeled and unlabeled MONPs, as these parameters are especially relevant for transport and uptake. Additionally, the impact of the core label on the photocatalytic activity should be determined, as this is a property that drives TiO_2 toxicity. The ratio of the metal label to the Ti within the labeled NPs should be reported, as well as the limits of detection and quantification.

Another case study we consider is the monitoring of ZnO NP uptake and translocation within an organism. Zn is an essential element for many organisms, and as such it is likely to be present prior to NP exposure. The use of a label allows for sensitive detection of the ZnO NPs against background levels of Zn, and can also provide the ability to visualize the ZnO NPs within the organism. As ZnO is a soluble MONP with ion-driven toxicity, it is important to be able to distinguish not only the ZnO NPs from the background Zn, but the Zn^{2+} ions after they are released through dissolution. Isotopic labeling techniques are ideal for these experiments because the Zn itself is specifically labeled and can be traced whether in ionic or particulate form. Radiolabeling is especially effective for examining MONP distribution among specific tissues and organs, as the sensitivity and ease of analysis offered by γ-spectrometry allows for the measurement of the small MONP quantities that may be present within a single biological compartment. ^{65}Zn also has the benefit of having an extremely long half-life for a radiolabel (244 days), sufficient even for long-term studies of chronic toxicity. If visualization is also desired, positron-emitting radiolabels like ^{18}F can be used to enable PET imaging, though these labels lack temporal stability due to the short half-life. Fluorescent dyes and QD labels can also be used

along with fluorescence microscopy. In the case of fluorescent dyes and QD labels, the solubility of ZnO NPs may make the label release and degrade in some compartments, limiting the capacity for imaging. For gavage, intravenous, or intratracheal doses of MONPs, the true administered dose must be determined by measuring the amount of MONPs remaining within the syringe, a task easily accomplished when a radiolabel is present. Characterization of radiolabeled MONPs used in this type of study should include a comparison of dissolution kinetics for the labeled and unlabeled ZnO NPs, tested in media with relevant pH and ionic strength values. It is also important to determine that no structural impact occurred during radiolabeling if direct activation was used to prepare the NPs. Size and crystal structure are two properties that could potentially be affected. The radioactivity of the produced MONPs should be reported, along with the limits of detection and quantification.

Table 5. Summary of labeling strategies.

	Fluorescent Dyes	Radioisotopes	Stable Isotopes	Core/Shell and Doping
Detection Sensitivity	• µg/L - g/L	• pg/L - ng/L	• ng/L - µg/L	• ng/L - mg/L
Label Stability	• Dye can degrade through photobleaching or interaction with ROS and enzymes • Poor applicability to soluble MONPs due to dye release • Low temporal and thermal stability	• Half-lives range from minutes-years • Label allows for tracking of released ions in soluble MONPs	• High temporal and thermal stability • Label allows for tracking of released ions in soluble MONPs	• Metal labels have high temporal and thermal stability • DNA labels have poor thermal stability • Poor applicability to soluble MONPs due to release of dopants or exposure of core
Cost and Equipment Requirements	• Most inexpensive synthesis and quantification • No specialized equipment	• Radioactive precursors and direct activation procedures are both expensive • Direct activation requires cyclotron/reactor source • Requires specialized equipment, laboratory, and waste disposal procedures.	• Expensive to synthesize and analyze • Low limits of detection require high-resolution ICP-MS	• Low – moderate expense for synthesis
Label Effects on MONP Properties	• Can alter rate of dissolution • Surface-attached dyes will alter MONP surface properties	• Some risk of thermally induced changes from direct activation • Recoil labeling embeds a foreign dopant into MONP, which can affect reactivity.	• Lowest possible impact to properties	• Can alter electronic properties • Dopant interacts with surrounding media and can affect surface chemistry • Core affects density
Ease of Label Incorporation and Quantification	• Cannot be applied to previously manufactured MONPs • Simple quantification and visualization • Tissues may need to be sliced to allow light penetration	• Can be applied to previously manufactured MONPs • Facile quantification in complex matrices with limited sample preparation	• Cannot be applied to previously manufactured MONPs • Care should be taken to avoid artefacts from acid digestion procedures or polyatomic interferences during analysis	• Cannot be applied to previously manufactured MONPs • Variety of quantification options for metal labels • QD core labels can be easily visualized

Conclusion

A variety of MONP labeling techniques have been developed for the purpose of studying MONPs in complex systems. When any of these labeling strategies is employed, characterization is critical to ensuring that the properties and behavior of the labeled MONP are representative of the unlabeled form. The decision of which technique to use will depend on the label stability and detection sensitivity requirements of the study, limitations imposed by equipment and cost, and the preservation of MONP properties that are critical to understanding the mechanism of behavior. Rigorous characterization and comparison of key properties to unlabeled MONPs is necessary for meaningful conclusions to be drawn from experiments that employ a labeling strategy. Currently, there are limited comparisons of key characteristics affecting MONP transport and toxicity. Improved reporting of label parameters, like the amount of the label incorporated into the MONPs, and the limits of detection and quantification, will help ensure that progress can continue to be made optimizing the preparation and utility of labeled MONPs. Ultimately, no one labeling technique will meet all research needs. The successful development and application of a variety of MONP labeling strategies enables experimental designs that reflect the complexity of the natural environment, better allowing for the determination of the mechanisms driving transport and toxicity.

Conflicts of Interest

There are no conflicts to declare.

Acknowledgments

The authors would like to thank Renata Behra for her insightful suggestions on this manuscript. We are grateful to National Science Foundation Awards 1255020 and 1314109-DGE for funding.

Works Cited

1 R. J. Aitken, M. Q. Chaudhry, A. B. A. Boxall and M. Hull, Manufacture and use of nanomaterials: current status in the UK and global trends, *Occup. Med.*, 2006, **56**, 300–306.

2 F. Piccinno, F. Gottschalk, S. Seeger and B. Nowack, Industrial production quantities and uses of ten engineered nanomaterials in Europe and the world, *J. Nanoparticle Res.*, 2012, **14**, 1109–1120.

3 P. A. Holden, F. Klaessig, R. F. Turco, J. H. Priester, C. M. Rico, H. Avila-Arias, M. Mortimer, K. Pacpaco and J. L. Gardea-Torresdey, Evaluation of exposure concentrations used in assessing manufactured nanomaterial environmental hazards: are they relevant?, *Environ. Sci. Technol.*, 2014, **48**, 10541–10551.

4 H. A. Jeng and J. Swanson, Toxicity of metal oxide nanoparticles in mammalian cells, *J. Environ. Sci. Heal. A*, 2006, **41**, 2699–2711.

5 M. Horie, K. Nishio, K. Fujita, S. Endoh, A. Miyauchi, Y. Saito, H. Iwahashi, K. Yamamoto, H. Murayama, H. Nakano, N. Nanashima, E. Niki and Y. Yoshida, Protein adsorption of ultrafine metal oxide and its influence on cytotoxicity toward cultured cells, *Chem. Res. Toxicol.*, 2009, **22**, 543–553.

6 K. Kasemets, A. Ivask, H. C. Dubourguier and A. Kahru, Toxicity of nanoparticles of ZnO, CuO and TiO_2 to yeast *Saccharomyces cerevisiae*, *Toxicol. Vitr.*, 2009, **23**, 1116–1122.

7 Y.-W. Huang, C. Wu and R. S. Aronstam, Toxicity of transition metal oxide nanoparticles: Recent insights from *in vitro* studies, *Materials*, 2010, **3**, 4842–4859.

8 S. M. Dizaj, F. Lotfipour, M. Barzegar-Jalali, M. H. Zarrintan and K. Adibkia, Antimicrobial activity of the metals and metal oxide nanoparticles, *Mater. Sci. Eng. C*, 2014, **44**, 278–284.

9 H. L. Karlsson, P. Cronholm, J. Gustafsson and L. Möller, Copper oxide nanoparticles are highly toxic: a comparison between metal oxide nanoparticles and carbon nanotubes, *Chem. Res. Toxicol*., 2008, **21**, 1726–1732.

10 Q. Wu, A. Nouara, Y. Li, M. Zhang, W. Wang, M. Tang, B. Ye, J. Ding and D. Wang, Comparison of toxicities from three metal oxide nanoparticles at environmental relevant concentrations in nematode *Caenorhabditis elegans*, *Chemosphere*, 2013, **90**, 1123–1131.

11 T. Xia, M. Kovochich, M. Liong, L. Mädler, B. Gilbert, H. Shi, J. I. Yeh, J. I. Zink, A. E. Nel, L. Ma, B. Gilbert, Ќ. H. Shi, J. I. Yeh, J. I. Zink, A. E. Nel, L. Mädler, B. Gilbert, H. Shi, J. I. Yeh, J. I. Zink and A. E. Nel, Comparison of the mechanism of toxicity of zinc oxide and cerium oxide nanoparticles based on dissolution and oxidative stress properties, *ACS Nano*, 2008, **2**, 2121–2134.

12 A. M. C. Ng, M. Y. Guo, Y. H. Leung, C. M. N. Chan, S. W. Y. Wong, M. M. N. Yung, A. P. Y. Ma, A. B. Djurišić, F. C. C. Leung, K. M. Y. Leung, W. K. Chan and H. K. Lee, Metal oxide nanoparticles with low toxicity, *J. Photochem. Photobiol. B*, 2015, **151**, 17–24.

13 K. Li, Y. Chen, W. Zhang, Z. Pu, L. Jiang and Y. Chen, Surface interactions affect the toxicity of engineered metal oxide nanoparticles toward *Paramecium*, *Chem. Res. Toxicol.*, 2012, **25**, 1675–1681.

14 K. Van Hoecke, J. T. K. Quik, J. Mankiewicz-Boczek, K. A. C. De Schamphelaere, A. Elsaesser, P. Van der Meeren, C. Barnes, G. McKerr, C. V. Howard, D. Van De Meent, K. Rydzyński, K. A. Dawson, A. Salvati, A. Lesniak, I. Lynch, G. Silversmit, B. De Samber, L. Vincze and C. R. Janssen, Fate and effects of CeO_2 nanoparticles in aquatic ecotoxicity tests, *Environ. Sci. Technol.*, 2009, **43**, 4537–4546.

15 L. K. Braydich-Stolle, J. L. Speshock, A. Castle, M. Smith, R. C. Murdock and S. M. Hussain, Nanosized aluminum altered immune function, *ACS Nano*, 2010, **4**, 3661–3670.

16 E. Kahn, M. Baarine, S. Pelloux, J. M. Riedinger, F. Frouin, Y. Tourneur and G. Lizard, Iron nanoparticles increase 7-ketocholesterol-induced cell death, inflammation, and oxidation on murine cardiac HL1-NB cells, *Int. J. Nanomedicine*, 2010, **5**, 185–195.

17 E. J. Park, H. Kim, Y. Kim, J. Yi, K. Choi and K. Park, Inflammatory responses may be induced by a single intratracheal instillation of iron nanoparticles in mice, *Toxicology*, 2010, **275**, 65–71.

18 O. Zeyons, A. Thill, F. Chauvat, N. Menguy, C. Cassier-Chauvat, C. Orear, J. Daraspe, M. Auffan, J. Rose and O. Spalla, Direct and indirect CeO_2 nanoparticles toxicity for *Escherichia coli* and *Synechocystis*, *Nanotoxicology*, 2009, **3**, 284–295.

19 A. Gajewicz, N. Schaeublin, B. Rasulev, S. Hussain, D. Leszczynska, T. Puzyn and J. Leszczynski, Towards understanding mechanisms governing cytotoxicity of metal oxides nanoparticles: hints from nano-QSAR studies, *Nanotoxicology*, 2015, **9**, 313–325.

20 Y. Li, W. Zhang, J. Niu and Y. Chen, Mechanism of photogenerated reactive oxygen species and correlation with the antibacterial properties of engineered metal-oxide nanoparticles, *ACS Nano*, 2012, **6**, 5164–5173.

21 A. B. Djurišić, Y. H. Leung, A. M. C. Ng, X. Y. Xu, P. K. H. Lee, N. Degger and R. S. S. Wu, Toxicity of metal oxide nanoparticles: mechanisms, characterization, and avoiding experimental artefacts, *Small*, 2015, **11**, 26–44.

22 M. Fernández-Garcia and J. A. Rodriguez, Metal Oxide Nanoparticles, in *Encyclopedia of inorganic chemistry*, ed. R.A. Scott, Wiley, New York, NY, 2006.

23 P. A. Cox, *The elements: their origin, abundance, and distribution*, Oxford University Press, New York, NY, 1989.

24 D. C. Adriano, *Trace elements in terrestrial environments: biogeochemistry, bioavailability and risk of metals*, Springer, New York, NY, 2001.

25 S. R. Taylor and S. McLennan, *The continental crust: Its composition and evolution*, Blackwells Scientific Publications, Palo Alto, CA, 1985.

26 K. W. Bruland, in *Chemical Oceanography*, eds. J. P. Riley and R. Chester, Academic Press, New York, NY, 1983, 157–220.

27 J. M. Martin and M. Meybeck, Elemental mass-balance of material carried by major world rivers, *Mar. Chem.,* 1979, **7**, 173–206.

28 H. J. M. Bowen, *Environmental chemistry of the elements*, Academic Press, New York, NY, 1979.

29 J. Gaillardet, J. Viers and B. Dupré, Trace elements in river waters, in *Treatise on geochemistry,* eds. H.D. Holland and K.K. Turekian, Elsevier Science, Oxford, 2003, 225-268.

30 F. Gottschalk, T. Sun and B. Nowack, Environmental concentrations of engineered nanomaterials: review of modeling and analytical studies, *Environ. Pollut.*, 2013, **181**, 287–300.

31 F. Gottschalk, T. Sonderer, R. W. Scholz and B. Nowack, Modeled environmental concentrations of engineered nanomaterials (TiO_2, ZnO, Ag, CNT, fullerenes) for different regions, *Environ. Sci. Technol.*, 2009, **43**, 9216–9222.

32 F. von der Kammer, P. L. Ferguson, P. A. Holden, A. Masion, K. R. Rogers, S. J. Klaine, A. A. Koelmans, N. Horne and J. M. Unrine, Analysis of engineered nanomaterials in complex matrices (environment and biota): general considerations and conceptual case studies, *Environ. Toxicol. Chem.*, 2012, **31**, 32–49.

33 K. Leopold, A. Philippe, K. Wörle and G. E. Schaumann, Analytical strategies to the determination of metal-containing nanoparticles in environmental waters, *Trends Anal. Chem.*, 2016, **84**, 107–120.

34 M. Baalousha, B. Stolpe and J. R. Lead, Flow field-flow fractionation for the analysis and characterization of natural colloids and manufactured nanoparticles in environmental systems: a critical review, *J. Chromatogr. A*, 2011, **1218**, 4078–4103.

35 B. Meermann, Field-flow fractionation coupled to ICP-MS: separation at the nanoscale, previous and recent application trends., *Anal. Bioanal. Chem.*, 2015, **407**, 2665–74.

36 A. Samontha, J. Shiowatana and A. Siripinyanond, Particle size characterization of titanium dioxide in sunscreen products using sedimentation field-flow fractionation-inductively coupled plasma-mass spectrometry, *Anal. Bioanal. Chem.*, 2011, **399**, 973–978.

37 J. Soto-Alvaredo, F. Dutschke, J. Bettmer, M. Montes-Bayón, D. Pröfrock and A. Prange, Initial results on the coupling of sedimentation field-flow fractionation (SdFFF) to inductively coupled plasma-tandem mass spectrometry (ICP-MS/MS) for the detection and characterization of TiO_2 nanoparticles, *J. Anal. At. Spectrom.*, 2016, **31**, 1549–1555.

38 A. R. Donovan, C. D. Adams, Y. Ma, C. Stephan, T. Eichholz and H. Shi, Detection of zinc oxide and cerium dioxide nanoparticles during drinking water treatment by rapid single particle ICP-MS methods, *Anal. Bioanal. Chem.*, 2016, **408**, 5137–5145.

39 Y. Dan, H. Shi, C. Stephan and X. Liang, Rapid analysis of titanium dioxide nanoparticles in sunscreens using single particle inductively coupled plasma-mass spectrometry, *Microchem. J.*, 2015, **122**, 119–126.

40 L. Fréchette-Viens, M. Hadioui and K. J. Wilkinson, Practical limitations of single particle ICP-MS in the determination of nanoparticle size distributions and dissolution: case of rare earth oxides, *Talanta*, 2017, **163**, 121–126.

41 S. Lee, X. Bi, R. B. Reed, J. F. Ranville, P. Herckes and P. Westerhoff, Nanoparticle size detection limits by single particle ICP-MS for 40 elements, *Environ. Sci. Technol.*, 2014, **48**, 10291–10300.

42 A. Makishima, X.-K. Zhu, N. S. Belshaw and R. K. O'Nions, Separation of titanium from silicates for isotopic ratio determination using multiple collector ICP-MS, *J. Anal. At. Spectrom.*, 2002, **17**, 1290–1294.

43 A. Praetorius, A. Gundlach-Graham, E. Goldberg, W. Fabienke, J. Navratilova, A. Gondikas, R. Kaegi, D. Günther, T. Hofmann and F. von der Kammer, Single-particle multi-element fingerprinting (spMEF) using inductively-coupled plasma time-of-flight mass spectrometry (ICP-TOFMS) to identify engineered nanoparticles against the elevated natural background in soils, *Environ. Sci. Nano*, 2017, **4**, 307-314.

44 A. Gondikas, F. Von Der Kammer, R. Kaegi, O. Borovinskaya, E. Neubauer, J. Navratilova, A. Praetorius, G. Cornelis and T. Hofmann, Where is the nano? Analytical approaches for the detection and quantification of TiO_2 engineered nanoparticles in surface waters, *Environ. Sci. Nano*, 2018, **5**, 313–326.

45 A. Weir, P. Westerhoff, L. Fabricius, K. Hristovski and N. von Goetz, Titanium dioxide nanoparticles in food and personal care products., *Environ. Sci. Technol.*, 2012, **46**, 2242–50.

46 P. J. Lu, S. C. Huang, Y. P. Chen, L. C. Chiueh and D. Y. C. Shih, Analysis of titanium dioxide and zinc oxide nanoparticles in cosmetics, *J. Food Drug Anal*., 2015, **23**, 587–594.

47 C.-Y. Jin, B.-S. Zhu, X.-F. Wang and Q.-H. Lu, Cytotoxicity of titanium dioxide nanoparticles in mouse fibroblast cells, *Chem. Res. Toxicol.*, 2008, **21**, 1871–1877.

48 D. R. Baer, D. J. Gaspar, P. Nachimuthu, S. D. Techane and D. G. Castner, Application of surface chemical analysis tools for characterization of nanoparticles, *Anal. Bioanal. Chem.*, 2010, **396**, 983–1002.

49 A. E. Pradas del Real, H. Castillo-Michel, R. Kaegi, C. Larue, W. de Nolf, J. Reyes-Herrera, R. Tucoulou, N. Findling, E. Salas-Colera and G. Sarret, Searching for relevant criteria to distinguish natural vs. anthropogenic TiO_2 nanoparticles in soils, *Environ. Sci. Nano*, 2018, **5**, 2853–2863.

50 J. Blechinger, R. Herrmann, D. Kiener, F. J. García-García, C. Scheu, A. Reller and C. Bräuchle, Perylene-labeled silica nanoparticles: synthesis and characterization of three novel silica nanoparticle species for live-cell imaging, *Small*, 2010, **6**, 2427–2435.

51 A. van Blaaderen and A. Vrij, Synthesis and characterization of colloidal dispersions of fluorescent, monodisperse silica spheres, *Langmuir*, 1992, **8**, 2921–2931.

52 A. Clemente, N. Moreno, M. P. Lobera, F. Balas and J. Santamaria, Fluorescently labelled SiO_2 nanoparticles as tracers in natural waters: dependence of detection limits on environmental conditions, *Environ. Sci. Nano*, 2016, **3**, 631–637.

53 R. P. Bagwe, C. Yang, L. R. Hilliard and W. Tan, Optimization of dye-doped silica nanoparticles prepared using a reverse microemulsion method, *Langmuir*, 2004, **19**, 8336–8342.

54 M. A. Kiser, H. Ryu, H. Jang, K. Hristovski and P. Westerhoff, Biosorption of nanoparticles to heterotrophic wastewater biomass, *Water Res.*, 2010, **44**, 4105–4114.

55 L. Otero-González, J. A. Field, I. A. C. Calderon, C. A. Aspinwall, F. Shadman, C. Zeng and R. Sierra-Alvarez, Fate of fluorescent core-shell silica nanoparticles during simulated secondary wastewater treatment, *Water Res.*, 2015, **77**, 170–178.

56 A. Zane, C. McCracken, D. A. Knight, T. Young, A. D. Lutton, J. W. Olesik, W. J. Waldman and P. K. Dutta, Uptake of bright fluorophore core-silica shell nanoparticles by biological systems, *Int. J. Nanomedicine*, 2015, **10**, 1547–1567.

57 S. Shahabi, L. Treccani and K. Rezwan, A comparative study of three different synthesis routes for hydrophilic fluorophore-doped silica nanoparticles, *J. Nanoparticle Res.*, 2016, **18**, 1–13.

58 E. Mahon, D. R. Hristov and K. a. Dawson, Stabilising fluorescent silica nanoparticles against dissolution effects for biological studies, *Chem. Commun.*, 2012, **48**, 7970–4972.

59 S. Quignard, G. Mosser, M. Boissière and T. Coradin, Long-term fate of silica nanoparticles interacting with human dermal fibroblasts, *Biomaterials*, 2012, **33**, 4431–4442.

60 E. Vitorge, S. Szenknect, J. M. F. Martins, V. Barthès, A. Auger, O. Renard and J.-P. Gaudet, Comparison of three labeled silica nanoparticles used as tracers in transport experiments in porous media. Part I: syntheses and characterizations, *Environ. Pollut.*, 2014, **184**, 605–612.

61 I. Chowdhury, D. M. Cwiertny and S. L. Walker, Combined factors influencing the aggregation and deposition of nano-TiO_2 in the presence of humic acid and bacteria, *Environ. Sci. Technol.*, 2012, **46**, 6968–6976.

62 A. A. Torrano and C. Bräuchle, Precise quantification of silica and ceria nanoparticle uptake revealed by 3D fluorescence microscopy, *Beilstein J. Nanotechnol.*, 2014, **5**, 1616–1624.

63 F. G. Strobl, F. Seitz, C. Westerhausen, A. Reller, A. A. Torrano, C. Bräuchle, A. Wixforth and M. F. Schneider, Intake of silica nanoparticles by giant lipid vesicles: influence of particle size and thermodynamic membrane state, *Beilstein J. Nanotechnol*., 2014, **5**, 2468–2478.

64 U. Resch-Genger, M. Grabolle, S. Cavaliere-Jaricot, R. Nitschke and T. Nann, Quantum dots versus organic dyes as fluorescent labels., *Nat. Methods*, 2008, **5**, 763–775.

65 J. Ovenstone and K. Yanagisawa, Effect of hydrothermal treatment of amorphous titania on the phase change from anatase to rutile during calcination, *Chem. Mater.*, 1999, **11**, 2770–2774.

66 C.-C. Wang and J. Y. Ying, Sol−gel synthesis and hydrothermal processing of anatase and rutile titania nanocrystals, *Chem. Mater.*, 1999, **11**, 3113–3120.

67 S. Quignard, Behaviour of silica nanoparticles in dermis-like cellularized collagen hydrogels, *Biomater. Sci.*, 2014, **2**, 484–492.

68 M. Al-Rawi, S. Diabaté and C. Weiss, Uptake and intracellular localization of submicron and nano-sized SiO_2 particles in *HeLa* cells, *Arch. Toxicol.*, 2011, **85**, 813–826.

69 J. Chen, H. Zhou, A. C. Santulli and S. S. Wong, Evaluating cytotoxicity and cellular uptake from the presence of variously processed TiO_2 nanostructured morphologies, *Chem. Res. Toxicol.* 2010, **23**, 871-879.

70 X. He, Y. Ma, M. Li, P. Zhang, Y. Li and Z. Zhang, Quantifying and imaging engineered nanomaterials *in vivo*: challenges and techniques, *Small*, 2013, **9**, 1482–1491.

71 T. Coradin, D. Eglin and J. Livage, The silicomolybdic acid spectrophotometric method and its application to silicate/biopolymer interaction studies, *Spectroscopy*, 2004, **18**, 567–576.

72 M. A. Rauf and S. Salman Ashraf, Survey of recent trends in biochemically assisted degradation of dyes, *Chem. Eng. J.*, 2012, **209**, 520–530.

73 Z. Zhang, Radiolabeling of nanoparticles, in *Toxicology of Nanomaterials*, eds. Y. Zhao, Z. Zhang and W. Feng, Wiley-VCH, Weinheim, Germany, 2016, 69–94.

74 C. Pérez-Campaña, V. Gómez-Vallejo, A. Martin, E. San Sebastián, S. E. Moya, T. Reese, R. F. Ziolo and J. Llop, Tracing nanoparticles in vivo: a new general synthesis of positron emitting metal oxide nanoparticles by proton beam activation, *Analyst*, 2012, **137**, 4902-4906.

75 U. Holzwarth, E. Bellido, M. Dalmiglio, J. Kozempel, G. Cotogno and N. Gibson, ^{7}Be-recoil radiolabelling of industrially manufactured silica nanoparticles, *J. Nanoparticle Res.*, 2014, **16**, 2574.

76 M. A. Malfatti, H. A. Palko, E. A. Kuhn and K. W. Turteltaub, Determining the pharmacokinetics and long-term biodistribution of SiO_2 nanoparticles *in vivo* using accelerator mass spectrometry, *Nano Lett.*, 2012, **12**, 5532–5538.

77 I. Cydzik, A. Bilewicz, K. Abbas, F. Simonelli, A. Bulgheroni, U. Holzwarth and N. Gibson, A novel method for synthesis of ^{56}Co-radiolabelled silica nanoparticles, *J. Nanoparticle Res.*, 2012, **14**, 1185.

78 S. H. Jung, K. Il Kim, J. H. Ryu, S. H. Choi, J. B. Kim, J. H. Moon and J. H. Jin, Preparation of radioactive core-shell type ^{198}Au@SiO_2 nanoparticles as a radiotracer for industrial process applications, *Appl. Radiat. Isot.*, 2010, **68**, 1025–1029.

79 J. Chen, S. D. Geraedts, C. Ouellet and B. Singh, Evaluation of half-life of ^{198}Au, *Appl. Radiat. Isot.*, 2011, **69**, 1064–1069.

80 H. Hildebrand, S. Schymura, U. Holzwarth, N. Gibson, M. Dalmiglio and K. Franke, Strategies for radiolabeling of commercial TiO_2 nanopowder as a tool for sensitive nanoparticle detection in complex matrices, *J. Nanoparticle Res.*, 2015, **17**, 278.

81 K. Abbas, I. Cydzik, R. Del Torchio, M. Farina, E. Forti, N. Gibson, U. Holzwarth, F. Simonelli and W. Kreyling, Radiolabelling of TiO_2 nanoparticles for radiotracer studies, *J. Nanoparticle Res.*, 2010, **12**, 2435–2443.

82 N. Gibson, U. Holzwarth, K. Abbas, F. Simonelli, J. Kozempel, I. Cydzik, G. Cotogno, A. Bulgheroni, D. Gilliland, J. Ponti, F. Franchini, P. Marmorato, H. Stamm, W. Kreyling, A. Wenk, M. Semmler-Behnke, S. Buono, L. MacIocco and N. Burgio, Radiolabelling of engineered nanoparticles for *in vitro* and *in vivo* tracing applications using cyclotron accelerators, *Arch. Toxicol.*, 2011, **85**, 751–773.

83 W. G. Kreyling, U. Holzwarth, N. Haberl, J. Kozempel, A. Wenk, S. Hirn, C. Schleh, M. Schäffler, J. Lipka, M. Semmler-Behnke and N. Gibson, Quantitative biokinetics of titanium dioxide nanoparticles after intratracheal instillation in rats: Part 3, *Nanotoxicology*, 2017, **11**, 454–464.

84 W. G. Kreyling, U. Holzwarth, C. Schleh, J. Kozempel, A. Wenk, N. Haberl, S. Hirn, M. Schäffler, J. Lipka, M. Semmler-Behnke and N. Gibson, Quantitative biokinetics of titanium dioxide nanoparticles after oral application in rats: Part 2, *Nanotoxicology*, 2017, **11**, 443–453.

85 W. G. Kreyling, U. Holzwarth, N. Haberl, J. Kozempel, S. Hirn, A. Wenk, C. Schleh, M. Schäffler, J. Lipka, M. Semmler-Behnke and N. Gibson, Quantitative biokinetics of titanium dioxide nanoparticles after intravenous injection in rats: Part 1, *Nanotoxicology*, 2017, **11**, 434–442.

86 C. W. Isaacson, L. Sigg, A. A. Ammann, J. Stadnicka-Michalak and K. Schirmer, Interactions of TiO_2 nanoparticles and the freshwater nematode *Plectus aquatilis*: particle properties, kinetic parameters and bioconcentration factors, *Environ. Sci. Nano*, 2017, **4**, 712–719.

87 C. Pérez-Campaña, F. Sansaloni, V. Gómez-Vallejo, Z. Baz, A. Martin, S. E. Moya, J. I. Lagares, R. F. Ziolo and J. Llop, Production of ^{18}F-labeled titanium dioxide nanoparticles by proton irradiation for biodistribution and biological fate studies in rats, *Part. Part. Syst. Charact.*, 2014, **31**, 134–142.

88 T.-K. Yeh, J.-K. Chen, C.-H. Lin, M.-H. Yang, C. S. Yang, F.-I. Chou, J.-J. Peir, M.-Y. Wang, W.-H. Chang, M.-H. Tsai, H.-T. Tsai and P. Lin, Kinetics and tissue distribution of neutron-activated zinc oxide nanoparticles and zinc nitrate in mice: effects of size and particulate nature, *Nanotechnology*, 2012, **23**, 085102.

89 W. M. Li and W. X. Wang, Distinct biokinetic behavior of ZnO nanoparticles in *Daphnia magna* quantified by synthesizing ^{65}Zn tracer, *Water Res.*, 2013, **47**, 895–902.

90 J. M. Cohen, R. Derk, L. Wang, J. Godleski, L. Kobzik, J. Brain and P. Demokritou, Tracking translocation of industrially relevant engineered nanomaterials (ENMs) across alveolar epithelial monolayers *in vitro*, *Nanotoxicology*, 2014, **8**, 216–225.

91 B. Huang, L. Xiao, L. Y. Yang, R. Ji and A. J. Miao, Facile synthesis of ^{55}Fe-labeled well-dispersible hematite nanoparticles for bioaccumulation studies in nanotoxicology, *Environ. Pollut.*, 2016, **213**, 801–808.

92 M. T. Zhu, W. Y. Feng, Y. Wang, B. Wang, M. Wang, H. Ouyang, Y. L. Zhao and Z. F. Chai, Particokinetics and extrapulmonary translocation of intratracheally instilled ferric oxide nanoparticles in rats and the potential health risk assessment, *Toxicol. Sci.*, 2009, **107**, 342–351.

93 B. Freund, U. I. Tromsdorf, O. T. Bruns, M. Heine, A. Giemsa, A. Bartelt, S. C. Salmen, N. Raabe, J. Heeren, H. Ittrich, R. Reimer, H. Hohenberg, U. Schumacher, H. Weller and P. Nielsen, A simple

and widely applicable method to ^{59}Fe-radiolabel monodisperse superparamagnetic iron oxide nanoparticles for *in vivo* quantification studies, *ACS Nano*, 2012, **6**, 7318–7325.

94 P. Marmorato, F. Simonelli, K. Abbas, J. Kozempel, U. Holzwarth, F. Franchini, J. Ponti, N. Gibson and F. Rossi, ^{56}Co-labelled radioactive Fe_3O_4 nanoparticles for *in vitro* uptake studies on Balb/3T3 and Caco-2 cell lines, *J. Nanoparticle Res.*, 2011, **13**, 6707–6716.

95 A. L. B. de Barros, A.-M. Chacko, J. L. Mikitsh, A. Al Zaki, A. Salavati, B. Saboury, A. Tsourkas and A. Alavi, Assessment of global cardiac uptake of radiolabeled iron oxide nanoparticles in apolipoprotein-E-deficient mice: implications for imaging cardiovascular inflammation, *Mol. Imaging Biol.*, 2013, **16**, 330–339.

96 S. Schymura, T. Fricke, H. Hildebrand and K. Franke, Elucidating the role of dissolution in CeO_2 nanoparticle plant uptake by smart radiolabeling, *Angew. Chemie Int. Ed.*, 2017, **56**, 7411–7414.

97 D. H. Oughton, T. Hertel-Aas, E. Pellicer, E. Mendoza and E. J. Joner, Neutron activation of engineered nanoparticles as a tool for tracing their environmental fate and uptake in organisms, *Environ. Toxicol. Chem.*, 2008, **27**, 1883.

98 F. Simonelli, P. Marmorato, K. Abbas, J. Ponti, J. Kozempel, U. Holzwarth, F. Franchini and F. Rossi, Cyclotron production of radioactive CeO_2 nanoparticles and their application for *in vitro* uptake studies, *IEEE Trans. Nanobioscience*, 2011, **10**, 44–50.

99 Z. Zhang, X. He, H. Zhang, Y. Ma, P. Zhang, Y. Ding and Y. Zhao, Uptake and distribution of ceria nanoparticles in cucumber plants, *Metallomics*, 2011, **3**, 816.

100 P. Zhang, X. He, Y. Ma, K. Lu, Y. Zhao and Z. Zhang, Distribution and bioavailability of ceria nanoparticles in an aquatic ecosystem model, *Chemosphere*, 2012, **89**, 530–535.

101 X. He, H. Zhang, Y. Ma, W. Bai, Z. Zhang, K. Lu, Y. Ding, Y. Zhao and Z. Chai, Lung deposition and extrapulmonary translocation of nano-ceria after intratracheal instillation., *Nanotechnology*, 2010, **21**, 285103.

102 S. Rojas, J. D. Gispert, S. Abad, M. Buaki-Sogo, V. M. Victor, H. Garcia and J. R. Herance, *In vivo* biodistribution of amino-functionalized ceria nanoparticles in rats using positron emission tomography, *Mol. Pharm.*, 2012, **9**, 3543–3550.

103 C. Pérez-Campaña, V. Gómez-Vallejo, M. Puigivila, A. Martín, T. Calvo-Fernández, S. E. Moya, R. F. Ziolo, T. Reese and J. Llop, Biodistribution of different sized nanoparticles assessed by positron emission tomography: a general strategy for direct activation of metal oxide particles, *ACS Nano*, 2013, **7**, 3498–3505.

104 H. P. Weise, W. Görner and M. Hedrich, Determination of elements by nuclear analytical methods, *Fresenius. J. Anal. Chem.*, 2001, **369**, 8–14.

105 U. Holzwarth, A. Bulgheroni, N. Gibson, J. Kozempel, G. Cotogno, K. Abbas, F. Simonelli and I. Cydzik, Radiolabelling of nanoparticles by proton irradiation: temperature control in nanoparticulate powder targets, *J. Nanoparticle Res.*, 2012, **14**, 880.

106 C. E. Crouthamel, F. Adams and R. Dams, in *Applied gamma-ray spectrometry*, eds. R. Belcher and H. Freiser, Elsevier and Pergamon Press, New York, 1970, 1–29.

107 S. Faucher and G. Lespes, Quantification of titanium from TiO_2 particles in biological tissue., *J. Trace Elem. Med. Biol.*, 2015, **32**, 40–44.

108 A. Laycock, B. Coles, K. Kreissig and M. Rehkämper, High precision $^{142}Ce/^{140}Ce$ stable isotope measurements of purified materials with a focus on CeO_2 nanoparticles, *J. Anal. At. Spectrom.*, 2016, **31**, 297–302.

109 T. W. May and R. H. Wiedmeyer, A Table of Polyatomic Interferences in ICP-MS, *At. Spectrosc*, 1998, **19**, doi:10.1039/c7ja00051k.

110 A. Laycock, B. Stolpe, I. Römer, A. Dybowska, E. Valsami-Jones, J. R. Lead and M. Rehkämper, Synthesis and characterization of isotopically labeled silver nanoparticles for tracing studies, *Environ. Sci. Nano*, 2014, **1**, 271.

111 P. L. Lee, B. C. Chen, G. Gollavelli, S. Y. Shen, Y. S. Yin, S. L. Lei, C. L. Jhang, W. R. Lee and Y. C. Ling, Development and validation of TOF-SIMS and CLSM imaging method for cytotoxicity study of ZnO nanoparticles in HaCaT cells, *J. Hazard. Mater.*, 2014, **277**, 3–12.

112 M. Kubicek, G. Holzlechner, A. K. Opitz, S. Larisegger, H. Hutter and J. Fleig, A novel ToF-SIMS operation mode for sub 100nm lateral resolution: application and performance, *Appl. Surf. Sci.*, 2014, **289**, 407–416.

113 F. Larner, Y. Dogra, A. Dybowska, J. Fabrega, B. Stolpe, L. J. Bridgestock, R. Goodhead, D. J. Weiss, J. Moger, J. R. Lead, E. Valsami-Jones, C. R. Tyler, T. S. Galloway and M. Rehkämper, Tracing bioavailability of ZnO nanoparticles using stable isotope labeling, *Environ. Sci. Technol.*, 2012, **46**, 12137–12145.

114 A. Laycock, A. Romero-freire, J. Najorka, C. Svendsen, C. A. M. Van Gestel and M. Rehka, novel multi-isotope tracer approach to test ZnO nanoparticle and soluble Zn bioavailability in joint soil exposures, *Environ. Sci. Technol.*, 2017, **51**, 12756-12763.

115 R. C. Merrifield and J. R. Lead, Preparation and characterization of three-layer, isotopically labelled core-shell nanoparticles; a tool for understanding mechanisms of bioavailability, *NanoImpact*, 2016, **2**, 54–60.

116 M. Croteau, D. J. Cain and C. C. Fuller, Novel and nontraditional use of stable isotope tracers to study metal bioavailability from natural particles, *Environ. Sci. Technol.*, 2013, **47**, 3424–3431.

117 M.-N. Croteau, D. J. Cain and C. C. Fuller, Assessing the dietary bioavailability of metals associated with natural particles: extending the use of the reverse labeling approach to zinc, *Environ. Sci. Technol.*, 2017, **51**, 2803–2810.

118 A. Bourgeault, C. Cousin, V. Geertsen, C. Cassier-Chauvat, F. Chauvat, O. Durupthy, C. Chanéac and O. Spalla, The challenge of studying TiO_2 nanoparticle bioaccumulation at environmental concentrations: crucial use of a stable isotope tracer, *Environ. Sci. Technol.*, 2015, **49**, 2451–2459.

119 M. N. Croteau, A. D. Dybowska, S. N. Luoma and E. Valsami-Jones, A novel approach reveals that zinc oxide nanoparticles are bioavailable and toxic after dietary exposures., *Nanotoxicology*, 2011, **5**, 79–90.

120 A. D. Dybowska, M. Croteau, S. K. Misra, D. Berhanu, S. N. Luoma, P. Christian, P. O'Brien and E. Valsami-Jones, Synthesis of isotopically modified ZnO nanoparticles and their potential as nanotoxicity tracers, *Environ. Pollut.*, 2011, **159**, 266–273.

121 P. E. Buffet, C. Amiard-Triquet, A. Dybowska, C. Risso-de Faverney, M. Guibbolini, E. Valsami-Jones and C. Mouneyrac, Fate of isotopically labeled zinc oxide nanoparticles in sediment and effects on two endobenthic species, the clam *Scrobicularia plana* and the ragworm *Hediste diversicolor*, *Ecotoxicol. Environ. Saf.*, 2012, **84**, 191–198.

122 B. Gulson, H. Wong, M. Korsch, L. Gomez, P. Casey, M. McCall, M. McCulloch, J. Trotter, J. Stauber and G. Greenoak, Comparison of dermal absorption of zinc from different sunscreen formulations and differing UV exposure based on stable isotope tracing, *Sci. Total Environ.*, 2012, **420**, 313–318.

123 F. Larner, B. Gulson, M. McCall, Y. Oytam and M. Rehkämper, An inter-laboratory comparison of high precision stable isotope ratio measurements for nanoparticle tracing in biological samples, *J. Anal. At. Spectrom.*, 2014, **29**, 471–477.

124 B. Gulson, M. McCall, F. Larner, Y. Oytam, L. Gomez and B. Baxter, Dermal absorption of Zn from ZnO particles in sunscreens applied to humans, *Toxicol. Lett.*, 2014, **229**, S191.

125 B. Gulson, M. McCall, M. Korsch, L. Gomez, P. Casey, Y. Oytam, A. Taylor, M. McCulloch, J. Trotter, L. Kinsley and G. Greenoak, Small amounts of zinc from zinc oxide particles in sunscreens applied outdoors are absorbed through human skin, *Toxicol. Sci.*, 2010, **118**, 140–149.

126 M. J. Osmond-McLeod, Y. Oytam, J. K. Kirby, L. Gomez-Fernandez, B. Baxter and M. J. McCall, Dermal absorption and short-term biological impact in hairless mice from sunscreens containing zinc oxide nano- or larger particles, *Nanotoxicology*, 2014, **8**, 72–84.

127 F. R. Khan, A. Laycock, A. Dybowska, F. Larner, B. D. Smith, P. S. Rainbow, S. N. Luoma, M. Rehkämper and E. Valsami-Jones, Stable isotope tracer to determine uptake and efflux dynamics of ZnO nano- and bulk particles and dissolved Zn to an estuarine snail, *Environ. Sci. Technol.*, 2013, **47**, 8532–8539.

128 F. Larner and M. Rehkämper, Evaluation of stable isotope tracing for ZnO nanomaterials-new constraints from high precision isotope analyses and modeling, *Environ. Sci. Technol.*, 2012, **46**, 4149–4158.

129 S. K. Misra, A. Dybowska, D. Berhanu, M. N. Croteau, S. N. Luoma, A. R. Boccaccini and E. Valsami-Jones, Isotopically modified nanoparticles for enhanced detection in bioaccumulation studies, *Environ. Sci. Technol.*, 2012, **46**, 1216–1222.

130 A. Thit, T. Ramskov, M.-N. N. Croteau and H. Selck, Biodynamics of copper oxide nanoparticles and copper ions in an oligochaete - part II: subcellular distribution following sediment exposure, *Aquat. Toxicol.*, 2016, **180**, 25–35.

131 T. Ramskov, A. Thit, M. N. Croteau and H. Selck, Biodynamics of copper oxide nanoparticles and copper ions in an oligochaete - part I: relative importance of water and sediment as exposure routes, *Aquat. Toxicol.*, 2015, **164**, 81–91.

132 M.-N. Croteau, S. K. Misra, S. N. Luoma and E. Valsami-Jones, Bioaccumulation and toxicity of CuO nanoparticles by a freshwater invertebrate after waterborne and dietborne exposures, *Environ. Sci. Technol.*, 2014, **48**, 10929–10937.

133 B. L. Beard and C. M. Johnson, Atom Exchange between Aqueous Fe(II) and Goethite: An Fe Isotope Tracer Study, *Environ. Sci. Technol.*, 2009, **43**, 1102–1107.

134 T. R. Reddy, A. J. Frierdich, B. L. Beard and C. M. Johnson, The effect of pH on stable iron isotope exchange and fractionation between aqueous Fe(II) and goethite, *Chem. Geol.*, 2015, **397**, 118–127.

135 B. Meermann, K. Wichmann, F. Lauer, F. Vanhaecke and T. A. Ternes, Application of stable isotopes and AF4/ICP-SFMS for simultaneous tracing and quantification of iron oxide nanoparticles in a sediment–slurry matrix, *J. Anal. At. Spectrom.*, 2016, **31**, 890–901.

136 V. Gomez, A. M. Balu, J. C. Serrano-Ruiz, S. Irusta, D. D. Dionysiou, R. Luque and J. Santamaría, Microwave-assisted mild-temperature preparation of neodymium-doped titania for the improved photodegradation of water contaminants, *Appl. Catal. A Gen.*, 2012, **441–442**, 47–53.

137 V. Gomez, A. Clemente, S. Irusta, F. Balas and J. Santamaria, Identification of TiO_2 nanoparticles using La and Ce as labels: application to the evaluation of surface contamination during the handling of nanosized matter, *Environ. Sci. Nano*, 2014, **1**, 496–503.

138 L.-J. A. Ellis, A. G. Papadiamantis, S. Weigel and E. Valsami-Jones, Synthesis and characterization of Zr- and Hf-doped nano-TiO_2 as internal standards for analytical quantification of nanomaterials in complex matrices, *R. Soc. Open Sci.*, 2018, **5**, 171884.

139 N. B. Saleh, D. J. Milliron, N. Aich, L. E. Katz, H. M. Liljestrand and M. J. Kirisits, Importance of doping, dopant distribution, and defects on electronic band structure alteration of metal oxide nanoparticles: Implications for reactive oxygen species, *Sci. Total Environ.*, 2016, **568**, 926–932.

140 V. Štengl, S. Bakardjieva and N. Murafa, Preparation and photocatalytic activity of rare earth doped TiO2 nanoparticles, *Mater. Chem. Phys.*, 2009, **114**, 217–226.

141 S. Veeranarayanan, A. C. Poulose, M. Sheikh Mohamed, Y. Nagaoka, S. Iwai, Y. Nakagame, S. Kashiwada, Y. Yoshida, T. Maekawa and D. Sakthi Kumar, Synthesis and application of luminescent single CdS quantum dot encapsulated silica nanoparticles directed for precision optical bioimaging, *Int. J. Nanomedicine*, 2012, **7**, 3769-3786.

142 N. Ma, A. F. Marshall, S. S. Gambhir and J. Rao, Facile synthesis, silanization, and biodistribution of biocompatible quantum dots, *Small*, **6**, 1520–1528.

143 A. R. Deline, W. M. Young and J. A. Nason, Gold core-labeled TiO_2 nanoparticles for tracking behavior in complex matrices: synthesis, characterization, and demonstration, *Environ. Sci. Nano*, 2018, **5**, 956–968.

144 J. Goebl, J. B. Joo, M. Dahl and Y. Yin, Synthesis of tailored Au@TiO_2 core-shell nanoparticles for photocatalytic reforming of ethanol, *Catal. Today*, 2014, **225**, 90–95.

145 X. M. Fan, W. J. Zou, R. A. Gu and J. L. Yao, Preparation of Au@SiO_2 core-shell nanoparticles and their surface-enhanced Raman spectra, *Chem. J. Chinese Univ.*, 2008, **29**, 130–134.

146 C. Chen, M. Shi, M. Cargnello, P. Fornasiero, C. B. Murray and R. J. Gorte, Au@TiO_2 core-shell nanostructures with high thermal stability, *Catal. Letters*, 2014, **144**, 1939–1945.

147 J. E. Lee, S. Bera, Y. S. Choi and W. I. Lee, Size-dependent plasmonic effects of M and M@SiO_2 (M = Au or Ag) deposited on TiO_2 in photocatalytic oxidation reactions, *Appl. Catal. B Environ.*, 2017, **214**, 15–22.

148 D. Paunescu, M. Puddu, J. O. B. Soellner, P. R. Stoessel and R. N. Grass, Reversible DNA encapsulation in silica to produce ROS-resistant and heat-resistant synthetic DNA 'fossils', *Nat. Protoc.*, 2013, **8**, 2440–2448.

149 R. N. Grass, J. Schälchli, D. Paunescu, J. O. B. Soellner, R. Kaegi and W. J. Stark, Tracking trace amounts of submicrometer silica particles in wastewaters and activated sludge using silica-encapsulated DNA barcodes, *Environ. Sci. Technol. Lett.*, 2014, **1**, 484–489.

150 C. A. Mora, D. Paunescu, R. N. Grass and W. J. Stark, Silica particles with encapsulated DNA as trophic tracers, *Mol. Ecol. Resour.*, 2015, **15**, 231–241.

151 D. Paunescu, C. A. Mora, L. Querci, R. Heckel, M. Puddu, B. Hattendorf, D. Günther and R. N. Grass, Detecting and number counting of single engineered nanoparticles by digital particle polymerase chain reaction, *ACS Nano*, 2015, **9**, 9564–9572.

152 K. T. Kim, S. J. Klaine, J. Cho, S. H. Kim and S. D. Kim, Oxidative stress responses of *Daphnia magna* exposed to TiO_2 nanoparticles according to size fraction, *Sci. Total Environ.*, 2010, **408**, 2268–2272.

153 J. Y. Roh, Y. K. Park, K. Park and J. Choi, Ecotoxicological investigation of CeO_2 and TiO_2 nanoparticles on the soil nematode *Caenorhabditis elegans* using gene expression, growth, fertility, and survival as endpoints, *Environ. Toxicol. Pharmacol.*, 2010, **29**, 167-72.

154 A. Simon-Deckers, S. Loo, M. Mayne-L'hermite, N. Herlin-Boime, N. Menguy, C. Reynaud, B. Gouget and M. Carrière, Size-, composition- and shape-dependent toxicological impact of metal oxide nanoparticles and carbon nanotubes toward bacteria, *Environ. Sci. Technol.*, 2009, **43**, 8423–8429.

155 M. Zhu, G. Nie, H. Meng, T. Xia, A. Nel and Y. Zhao, Physicochemical properties determine nanomaterial cellular uptake, transport, and fate, *Acc. Chem. Res.*, 2013, **46**, 622–631.

156 V. Filipe, A. Hawe and W. Jiskoot, Critical evaluation of nanoparticle tracking analysis (NTA) by NanoSight for the measurement of nanoparticles and protein aggregates, *Pharm. Res.*, 2010, **27**, 796–81.

157 M. Batzill, Fundamental aspects of surface engineering of transition metal oxide photocatalysts, *Energy Environ. Sci.*, 2011, **4**, 3275.

158 T. Luttrell, S. Halpegamage, J. Tao, A. Kramer, E. Sutter and M. Batzill, Why is anatase a better photocatalyst than rutile? Model studies on epitaxial TiO_2 films., *Sci. Rep.*, 2014, **4**, 4043.

159 G. Oberdörster, E. Oberdörster and J. Oberdörster, Nanotoxicology: an emerging discipline evolving from studies of ultrafine particles, *Environ. Health Perspect.*, 2005, **113**, 823-839.

160 A. J. Kennedy, M. S. Hull, S. Diamond, M. Chappell, A. J. Bednar, J. G. Laird, N. L. Melby and J. A. Steevens, Gaining a critical mass: a dose metric conversion case study using silver nanoparticles, *Environ. Sci. Technol.*, 2015, **49**, 12490–12499.

161 M. Hull, A. J. Kennedy, C. Detzel, P. Vikesland and M. A. Chappell, Moving beyond mass: the unmet need to consider dose metrics in environmental nanotoxicology studies, *Environ. Sci. Technol.*, 2012, **46**, 10881–10882.

162 R. P. Carney, J. Y. Kim, H. Qian, R. Jin, H. Mehenni, F. Stellacci and O. M. Bakr, Determination of nanoparticle size distribution together with density or molecular weight by 2D analytical ultracentrifugation., *Nat. Commun.*, 2011, **2**, 335.

163 V. Mittal and M. D. Lechner, Size and density dependent sedimentation analysis of advanced nanoparticle systems, *J. Colloid Interface Sci.*, 2010, 346, 378-383.

164 V. K. Sharma, Aggregation and toxicity of titanium dioxide nanoparticles in aquatic environment—a review, *J Environ Sci Health A Tox Hazard Subst Environ Eng*, 2009, **4414**, 1093–4529.

165 S. M. Louie, R. D. Tilton and G. V. Lowry, Critical review: impacts of macromolecular coatings on critical physicochemical processes controlling environmental fate of nanomaterials, *Environ. Sci. Nano*, 2016, **3**, 283–310.

166 D. P. Stankus, S. E. Lohse, J. E. Hutchison and J. a. Nason, Interactions between natural organic matter and gold nanoparticles stabilized with different organic capping agents., *Environ. Sci. Technol.*, 2011, **45**, 3238–3244.

167 M. C. Surette and J. A. Nason, Effects of surface coating character and interactions with natural organic matter on the colloidal stability of gold nanoparticles, *Environ. Sci. Nano*, 2016, **3**, 1144–1152.

168 R. Huber and S. Stoll, Protein affinity for TiO_2 and CeO_2 manufactured nanoparticles. From ultra-pure water to biological media, *Colloids Surfaces A Physicochem. Eng. Asp.*, 2018, **553**, 425–431.

169 A. Márquez, T. Berger, A. Feinle, N. Hüsing, M. Himly, A. Duschl and O. Diwald, Bovine serum albumin adsorption on TiO_2 colloids: the effect of particle agglomeration and surface composition, *Langmuir*, 2017, **33**, 2551–2558.

170 G. V. Lowry, K. B. Gregory, S. C. Apte and J. R. Lead, Transformations of nanomaterials in the environment, *Environ. Sci. Technol.*, 2012, **46**, 6893–6899.

171 H. J. Sung, S. R. Al-Abed and T. Luxton, Influence of carboxymethyl cellulose for the transport of titanium dioxide nanoparticles in clean silica and mineral-coated sands, *Environ. Sci. Technol.*, 2009, **43**, 4954-4959.

172 M. D. Torelli, R. A. Putans, Y. Tan, S. E. Lohse, C. J. Murphy and R. J. Hamers, Quantitative determination of ligand densities on nanomaterials by X-ray photoelectron spectroscopy, *ACS Appl. Mater. Interfaces*, 2015, **7**, 1720–1725.

173 D. H. Tsai, M. Davila-Morris, F. W. Delrio, S. Guha, M. R. Zachariah and V. A. Hackley, Quantitative determination of competitive molecular adsorption on gold nanoparticles using attenuated total reflectance-fourier transform infrared spectroscopy, *Langmuir*, 2011, **27**, 9302-9313.

174 A. L. Capriotti, G. Caracciolo, C. Cavaliere, V. Colapicchioni, S. Piovesana, D. Pozzi and A. Laganà, Analytical methods for characterizing the nanoparticle-protein corona, *Chromatographia*, 2014, **77**, 755–769.

175 G. V. Lowry, R. J. Hill, S. Harper, A. F. Rawle, C. O. Hendren, F. Klaessig, U. Nobbmann, P. Sayre and J. Rumble, Guidance to improve the scientific value of zeta-potential measurements in nanoEHS, *Environ. Sci. Nano*, 2016, **3**, 953–965.

176 Y. Xiao and M. R. Wiesner, Characterization of surface hydrophobicity of engineered nanoparticles, *J. Hazard. Mater.*, 2012, **215–216**, 146–151.

177 Y. Xiao and M. R. Wiesner, Transport and retention of selected engineered nanoparticles by porous media in the presence of a biofilm, *Environ. Sci. Technol.*, 2013, **47**, 2246–2253.

178 L. Crandon, Addressing persistent challenges in nanotoxicology exposures: techniques for *in situ* characterization, Oregon State University, 2018.

179 N. K. Geitner, S. M. Marinakos, C. Guo, N. O'Brien and M. R. Wiesner, Nanoparticle surface affinity as a predictor of trophic transfer, *Environ. Sci. Technol.*, 2016, **50**, 6663-6669.

180 N. K. Geitner, N. J. O'Brien, A. A. Turner, E. J. Cummins and M. R. Wiesner, Measuring nanoparticle attachment efficiency in complex systems, *Environ. Sci. Technol.*, 2017, **51**, 13288-13294.

181 H. F. Lecoanet, J. Y. Bottero and M. R. Wiesner, Laboratory assessment of the mobility of nanomaterials in porous media, *Environ. Sci. Technol.*, 2004, **38**, 5164-5169.

182 K. L. Chen and M. Elimelech, Aggregation and deposition kinetics of fullerene (C60) nanoparticles, *Langmuir*, 2006, **22**, 10994-11001.

183 H. Zhang, Z. Ji, T. Xia, H. Meng, C. Low-Kam, R. Liu, S. Pokhrel, S. Lin, X. Wang, Y. P. Liao, M. Wang, L. Li, R. Rallo, R. Damoiseaux, D. Telesca, L. Mädler, Y. Cohen, J. I. Zink and A. E. Nel, Use of metal oxide nanoparticle band gap to develop a predictive paradigm for oxidative stress and acute pulmonary inflammation, *ACS Nano*, 2012, **6**, 4349–4368.

184 C. Corredor, M. D. Borysiak, J. Wolfer, P. Westerhoff and J. D. Posner, colorimetric detection of catalytic reactivity of nanoparticles in complex matrices, *Environ. Sci. Technol.*, 2015, **49**, 3611–3618.

185 L. M. Gilbertson, E. M. Albalghiti, Z. S. Fishman, F. Perreault, C. Corredor, J. D. Posner, M. Elimelech, L. D. Pfefferle and J. B. Zimmerman, Shape-dependent surface reactivity and antimicrobial activity of nano-cupric oxide, *Environ. Sci. Technol.*, 2016, **50**, 3975–3984.

186 J. Zhao and M. Riediker, Detecting the oxidative reactivity of nanoparticles: a new protocol for reducing artifacts, *J. Nanoparticle Res.*, 2014, **16**, 2493.

187 A. M. Wormington, J. Coral, M. M. Alloy, C. L. Delmarè, C. M. Mansfield, S. J. Klaine, J. H. Bisesi and A. P. Roberts, Effect of natural organic matter on the photo-induced toxicity of titanium dioxide nanoparticles, *Environ. Toxicol. Chem.*, 2017, **36**, 1661–1666.

188 W. Hou and S. B. Cronin, A review of surface plasmon resonance-enhanced photocatalysis, *Adv. Funct. Mater.*, 2013, **23**, 1612–1619.

189 Y. Tian and T. Tatsuma, Plasmon-induced photoelectrochemistry at metal nanoparticles supported on nanoporous TiO_2, *Chem. Commun.*, 2004, **0**, 1810-1811.

190 H. Choi, W. T. Chen and P. V. Kamat, Know thy nano neighbor. Plasmonic versus electron charging effects of metal nanoparticles in dye-sensitized solar cells, *ACS Nano*, 2012, **6**, 4418–4427.

191 A. Zaleska, Doped-TiO_2: a review, *Recent Patents on Engineering*, 2008, **2**, 157–164.

192 S. Linic, P. Christopher and D. B. Ingram, Plasmonic-metal nanostructures for efficient conversion of solar to chemical energy, *Nat. Mater.*, 2011, **10**, 911–921.

193 M. E. Pettitt and J. R. Lead, Minimum physicochemical characterisation requirements for nanomaterial regulation, *Environ. Int.*, 2013, **52**, 41–50.

194 D. G. Thomas, S. Gaheen, S. L. Harper, M. Fritts, F. Klaessig, E. Hahn-Dantona, D. Paik, S. Pan, G. A. Stafford, E. T. Freund, J. D. Klemm and N. A. Baker, ISA-TAB-Nano: a specification for sharing nanomaterial research data in spreadsheet-based format, *BMC Biotechnol.*, 2013, **13**, doi: 10.1186/1472-6750-13-2.

195 A. Bour, F. Mouchet, S. Cadarsi, J. Silvestre, L. Verneuil, D. Baqué, E. Chauvet, J.-M. Bonzom, C. Pagnout, H. Clivot, I. Fourquaux, M. Tella, M. Auffan, L. Gauthier and E. Pinelli, Toxicity of CeO_2 nanoparticles on a freshwater experimental trophic chain: A study in environmentally relevant conditions through the use of mesocosms, *Nanotoxicology*, 2016, **10**, 245-255.

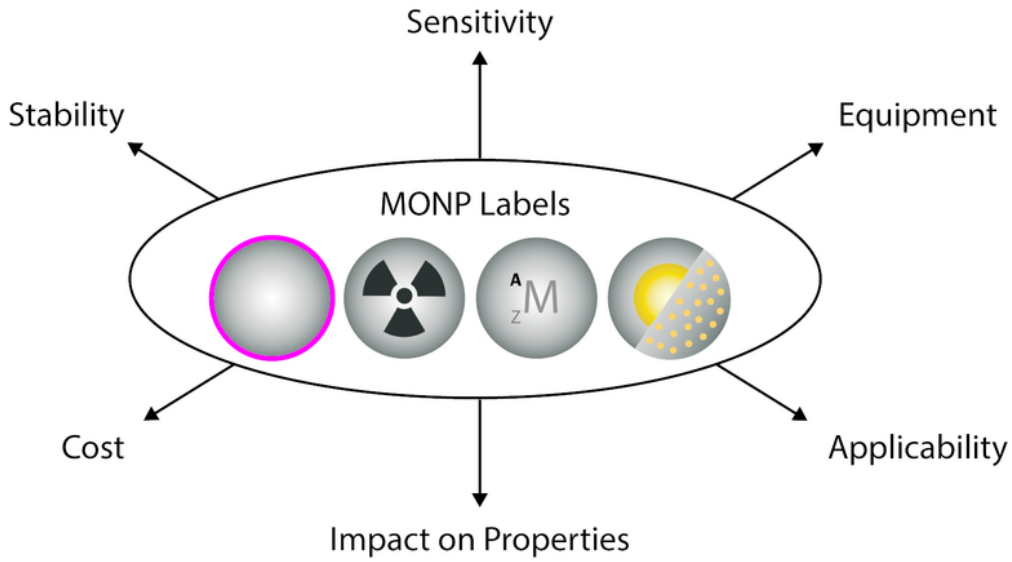

65x36mm (300 x 300 DPI)